Journal of Sound and Vibration 327 (2009) 529–556

Contents lists available at ScienceDirect

Journal of Sound and Vibration

journal homepage: www.elsevier.com/locate/jsvi

# Transmission of sonic booms into a rectangular room with a plaster–wood wall using a modal – Interaction model

Marcel C. Remillieux, Ricardo A. Burdisso *, Georg Reichard

*Mechanical Engineering Department, Virginia Polytechnic Institute and State University, Blacksburg, VA 24061, USA*

ARTICLE INFO

*Article history:*
Received 11 February 2009
Received in revised form
13 July 2009
Accepted 14 July 2009
Handling Editor: S. Bolton
Available online 7 August 2009

ABSTRACT

As a first step in the development of a model for predicting the noise transmission of sonic booms inside buildings, a numerical solution for the transmission of a shock wave with an arbitrary time history into a rectangular room with a plaster–wood wall is investigated. The dynamics of this fluid–structure system, including their interaction, is computed in the time domain using a modal-interaction method. The formulation of the problem, illustrative numerical results, and a parametric study are presented. The experimental effort dedicated to validating the numerical formulation is also presented. A speaker generating sonic booms with various durations is used to structurally load a plaster–wood wall mounted in the opening of a cinderblock room. The measured wall vibration and pressures at several locations inside the room are compared to the numerical predictions, showing a fairly good agreement overall. Results from this study can potentially be used by aircraft designers to minimize the noise impact in residential houses.



## 1. Introduction

Overland supersonic flights of commercial aircraft are currently banned due the strength of the sonic booms generated. The design of a commercial supersonic aircraft must account for the boom produced at the ground level, and in particular the noise exposure inside residential buildings. In that regard, a computer package that could predict the vibro-acoustic response of a building would be very useful to the aircraft designer, as an alternative to the prohibitive cost of flight testing. The work presented in this paper is directly related to this application.

The problem of the transmission of sonic booms inside enclosures was first investigated by Pretlove [1]. A solution was found for the free structural response of a panel backed by a closed cavity using modal decomposition. The approach was later extended to the structural response of the panel excited by a random pressure loading [2]. The problem was solved in the frequency domain by taking the Fourier transform of the structural dynamic equation. Finally, this approach was simplified by Pretlove and Craggs [3] to predict the fundamental mode of the coupled system.

The analysis of the dynamic response of a plaster–wood wall subjected to an arbitrary pressure loading has been carried out by Wahba [4]. The wall was considered as an assembly of elements with different material properties. Assuming a series solution of the displacement, Lagrange equations were used to formulate the equations of motion of the assembly (wall). These equations were then used to predict the transmission of sonic booms through the wall [5]. The dynamics of

* Corresponding author.
*E-mail addresses:* mremilli@vt.edu (M.C. Remillieux), rburdiss@vt.edu (R.A. Burdisso), reichard@vt.edu (G. Reichard).

0022-460X/$ - see front matter © 2009 Elsevier Ltd. All rights reserved.
doi:10.1016/j.jsv.2009.07.010

the plaster–wood wall was also investigated using finite elements (consistent- and lumped-mass formulations) to obtain solutions for arbitrary wall geometries [6].

The formulation proposed by Wahba [4,5] is very detailed and provides numerical solutions for the wall dynamics that agree very well with experiments. The work presented here differs from Wahba's in three main aspects. Firstly, the plaster–wood wall is treated as a homogeneous orthotropic plate. This approach is simpler and potentially more practical. Secondly, the fluid–structure interaction is fully coupled using the modal-interaction model developed by Fahy [7] for the transmission of a wave with arbitrary shape through a panel backed by a cavity. The modal approach is well suited to this problem as most of the acoustic energy of a typical sonic boom is contained in the very low frequency range and thus a relatively small number of structural and acoustic modes need to be considered. Thirdly, a detailed parametric study is undertaken in this work to assess the effects of the incident wave parameters and effects of the wall and room dimensions on the vibro-acoustic response.

Due to the relatively high operation costs, sonic booms are rarely generated by flying supersonic aircraft for research purposes. Sonic boom simulators are usually preferred. The most common sonic boom simulators encountered are horns, explosive charges, and speakers. Speakers have the advantage of reproducing many pressure signatures without the experimental efforts required from other sonic boom simulators such as explosives or horns. With appropriate frequency and phase compensation, those devices are capable of producing a wide range of overpressures, rise times, and stimuli durations. However, such systems may fall short of overpressure amplitude. Small chambers equipped with arrays of loudspeakers have been used extensively in studies of human response to impulsive noises, including sonic booms [8,9–11]. Arrays of speakers have also been used for structural forcing [12]. In this paper, sonic booms were generated with a speaker, providing data to validate the numerical formulation.

This paper is organized as follows: Section 2 describes the numerical formulation of the problem. Section 3 presents numerical results for illustrative examples. In this section, the effect of the shock-wave orientation and effect of vibro-acoustic coupling on the system response are also investigated. Section 4 summarizes results of a parametric study involving the effects of wave duration and shape, and effects of the wall and room dimensions on the system response. Section 5 describes the experimental effort including the experimental apparatus, results from a modal analysis of the wall, and a comparison of the numerical predictions with the experimental data. Section 6 concludes.

## 2. Numerical formulation

Consider the structure shown in Fig. 1 consisting of an elastic plate backed by a rigid rectangular enclosure. This system, initially at rest, is suddenly excited by a shock wave propagating along an arbitrary direction. The analysis of this problem may be divided into three main aspects, the computation of the time pressure loading on the structure, the structural response, and the acoustic response inside the room.

The pressure loading on the plate is a traveling wave with an arbitrary time history, not necessarily the ideal N-wave observed for high intensity sonic booms. As a result of the external loading, the plate vibrates and radiates sound into the enclosure. The pressure fluctuation inside the room creates an additional pressure loading on the plate, which causes the structure dynamics and interior acoustics to be fully coupled. The structural displacement is expressed in terms of the "in vacuo" modes of vibration of the plate with simply supported boundary conditions. The acoustic pressure inside the enclosure may also be formulated using series solutions, in terms of the acoustic modes of a room with rigid boundary conditions. Advantage is then taken of the orthogonality of the modes to obtain two finite sets of modal equations.

Fig. 2 is a schematic of the structure and the coordinate system. The dynamics of the plate is described in the $(x_s, y_s, z_s)$ Cartesian coordinate system. The plate is assumed to be uniform orthotropic with a mass per unit area $m_s$, thickness $h$, and

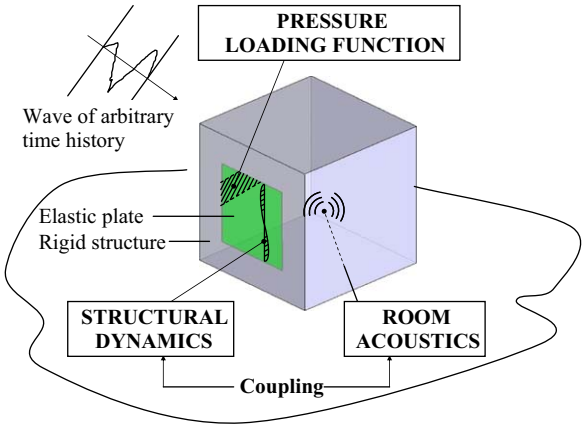


**Fig. 1.** Problem description.

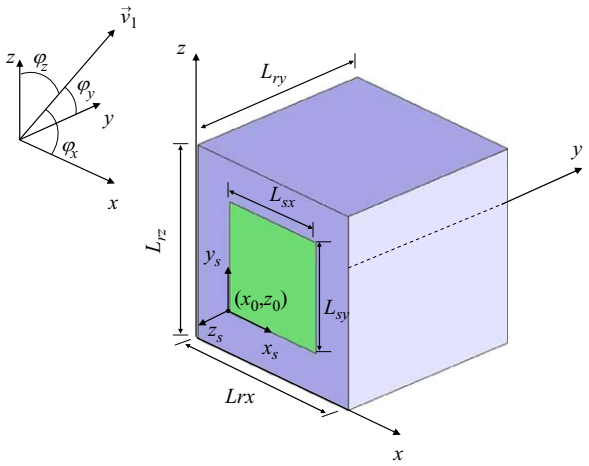


**Fig. 2.** The structure and coordinate systems.

dimensions $L_{sx}$ and $L_{sy}$ along the $x_s$- and $y_s$-directions, respectively. The acoustics inside the room is described in the $(x, y, z)$ Cartesian coordinate system. The room is a rectangular enclosure with dimensions $L_{rx}$, $L_{ry}$, and $L_{rz}$ along the $x$-, $y$-, and $z$-directions, respectively. The wave front exciting the plate propagates along $\vec{v}_1$, whose orientation is described by the set of directional angles $\varphi_x$, $\varphi_y$, and $\varphi_z$. The wave travels with a velocity $c\vec{v}_1$, where $c$ is the speed of sound in air.

### 2.1. Pressure loading

The computation of the pressure loading over the plate surface is greatly simplified by considering the wall as an infinite rigid plane surface. For the case of a shock wave with pressure time history $p_{sw}(t)$ arriving at normal incidence, the external pressure loading $p_{ext}(x_s, y_s, t)$ on the plate is uniform, and thus, simply a function of time,

$$p_{ext}(x_s, y_s, t) = 2p_{sw}(t) \tag{1}$$

where the factor 2 accounts for the pressure doubling due to the reflected wave on the plate surface. For the case of a wave arriving at oblique incidence, the external pressure loading on the plate also depends on the position on the plate surface. The wavefront arriving at the origin of the plate $(x_s, y_s) = (0,0)$ at time $t = 0$ produces the same excitation at an arbitrary point on the plate surface at time $t = \tau(x_s, y_s)$. The delay $\tau$ depends on the wave orientation relative to the plate, wave speed, and position on the plate surface, and may be expressed as

$$\tau(x_s, y_s) = \sqrt{\left(\left(\frac{x_s \cos(\varphi_x)}{c}\right)^2 + \left(\frac{y_s \cos(\varphi_z)}{c}\right)^2\right)} \tag{2}$$

For a wave at oblique incidence, the external pressure loading on the plate is

$$p_{ext}(x_s, y_s, t) = 2p_{sw}(t - \tau(x_s, y_s)) \tag{3}$$

Pressure doubling does not exactly occur over the plate surface for mainly two reasons. Firstly, diffraction of the incident wave over the edges and corners of the enclosure in which the plate is embedded will produce an additional pressure loading over the plate surface. Secondly, the plate is not rigid but has elastic and inertial properties. As the plate vibrates it creates an additional scattered field, commonly called radiated field. A boundary element code would provide the solutions for these additional pressure fields over the plate surface. However, the main objective of this paper is to present a formulation to compute the fluid–structure interaction of a plate backed by an enclosure and understand the physical mechanisms involved in that interaction. The pressure-doubling assumption provides a simple expression for the purpose of numerical simulations.

### 2.2. Eigenvalue problem

A plaster–wood wall used in a typical construction consists essentially of stiffeners sandwiched between plaster and wood (oriented strand board) panels, with insulation filling the cavity. Fig. 3 shows a schematic of such a wall. Stiffened plates differ from uniform plates in that their properties are directional, i.e. their bending rigidity about one axis is not necessarily the same as the bending rigidity about a perpendicular axis. Results from modal tests presented in Section 5 indicate that it is a reasonable assumption to consider the wall as a uniform orthotropic plate.

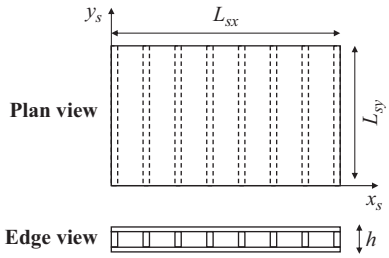


**Fig. 3.** Schematic of a plaster–wood wall.

The deflection of the plate can be expressed in terms of a summation over the "in vacuo" modes of vibration of the plate as

$$w(x_s, y_s, t) \approx \sum_{n=1}^{N_s} q_n(t)\phi_n(x_s, y_s) \tag{4}$$

where $N_s$ is the number of modes included in the expansion, $q_n(t)$ is the modal displacement, and $\phi_n(x_s, y_s)$ are the mode shapes of the plate. The mode shapes of a uniform orthotropic plate resting on simple supports are a product of sine functions given by

$$\phi_n(x_s, y_s) = A_{(n_x,n_y)} \sin\left(\frac{n_x\pi}{L_{sx}}x_s\right) \sin\left(\frac{n_y\pi}{L_{sy}}y_s\right) \tag{5}$$

where $n \to (n_x, n_y)$ and $A_{(n_x,n_y)}$ is a normalization factor. If the thickness of the plate is much smaller than the other two dimensions, which is usually the case for the walls of a building, then shear may be neglected. In this case, the natural angular frequency of a rectangular orthotropic plate may be approximated as [13]

$$\omega_n^s = \frac{\pi^2}{\sqrt{m_s}}\left[D_x\left(\frac{n_x}{L_{sx}}\right)^4 + D_y\left(\frac{n_y}{L_{sy}}\right)^4 + \left(\frac{2n_x^2n_y^2}{L_{sx}^2L_{sy}^2}\right)D_{xy}\right]^{1/2} \tag{6}$$

where $D_x$, $D_y$, and $D_{xy}$ are orthotropic constants. These constants are defined as (when shear is neglected)

$$\begin{cases} D_x = \dfrac{E_x h^3}{12(1-v_x v_y)} \\ D_y = \dfrac{E_y h^3}{12(1-v_x v_y)} \\ D_{xy} = D_x v_y \end{cases} \tag{7}$$

where $E_x$ and $E_y$ are the Young moduli, and $v_x$ and $v_y$ are the Poisson ratios in the $x_s$- and $y_s$-directions, respectively. The structural mode shapes satisfy the orthogonality conditions,

$$\int\int_S \phi_{n'} m_s \phi_n \, \mathrm{d}s = \delta_{nn'} \tag{8}$$

$$\int\int_S \phi_{n'} D\nabla^4[\phi_n] \, \mathrm{d}s = \omega_n^{s^2}\delta_{nn'} \tag{9}$$

The pressure inside the room may be expressed in terms of a summation over the acoustic modes of the room,

$$p(x, y, z, t) \approx \sum_{m=0}^{N_a} a_m(t)\psi_m(x, y, z) \tag{10}$$

where $N_a$ is the number of modes included in the expansion and $a_m(t)$ is the modal pressure. The mode shapes and natural angular frequencies $\omega_m^a$ of the room with hard walls are given by [14]

$$\psi_m(x, y, z) = R_{(m_x,m_y,m_z)} \cos\left(\frac{m_x\pi}{L_{rx}}x\right) \cos\left(\frac{m_y\pi}{L_{ry}}y\right) \cos\left(\frac{m_z\pi}{L_{rz}}z\right) \tag{11}$$

$$\omega_m^a = c\pi\sqrt{\left(\frac{m_x}{L_{rx}}\right)^2 + \left(\frac{m_y}{L_{ry}}\right)^2 + \left(\frac{m_z}{L_{rz}}\right)^2} \tag{12}$$

where $m \rightarrow (m_x, m_y, m_z)$ and $R_{(m_x,m_y,m_z)}$ is a normalization factor. The acoustic modes of the room are normalized to have a mean volume average of 1. The acoustic mode shapes satisfy the orthogonality conditions

$$\int\int\int_V \psi_m \psi_{m'} \, \mathrm{d}v = \delta_{mm'} V \tag{13}$$

$$\int\int\int_V \psi_{m'} \nabla^2 \psi_m \, \mathrm{d}v = -k_m^2 \delta_{mm'} V \tag{14}$$

where $k_m = \omega_m^a / c$, and $V$ is the volume of the room.

### 2.3. Fluid–structure interaction

The pressure inside the room is a solution of the inhomogeneous wave equation

$$\nabla^2 p - \frac{1}{c^2} \frac{\partial^2 p}{\partial t^2} = -\frac{\partial^2 m_d}{\partial t^2} \tag{15}$$

where $m_d$ is the mass displaced per unit volume. The plate deflection $w$ is assumed to be directed toward the fluid volume, which yields

$$\frac{\partial m_d}{\partial t} = 2\rho_r \frac{\partial w(x_s, y_s)}{\partial t} \delta(\xi - \xi_s) \tag{16}$$

where $\rho_r$ is the mass density of the air confined in the room. Replacing this expression into Eq. (15) leads to

$$\nabla^2 p - \frac{1}{c^2} \frac{\partial^2 p}{\partial t^2} = -2\rho_r \frac{\partial^2 w}{\partial t^2} \delta(\xi - \xi_s) \tag{17}$$

In the above equation, the pressure and the plate deflection may be expressed as summations over the acoustic modes of a room with hard walls and the "in vacuo" structural modes of the plate, respectively, which yields

$$\sum_m a_m \nabla^2 \psi_m - \left(\frac{1}{c}\right)^2 \sum_m \ddot{a}_m \psi_m = -2\rho_r \sum_n \ddot{q}_n \phi_n \delta(\xi - \xi_s) \tag{18}$$

Using the orthogonality properties of the acoustic modes, a finite set of ordinary differential equations is obtained that describes the modal dynamics of the pressure inside the room,

$$\omega_m^{a^2} a_m + \ddot{a}_m = \frac{2\rho_r c^2}{V} \sum_n \ddot{q}_n \int_S \psi_m \phi_n \, \mathrm{d}s \tag{19}$$

The above equation can be rewritten in terms of the velocity potential $\Phi$ to reduce the order of the time derivative on the right hand side. The velocity potential has the same mode shape functions and the same natural frequencies as the pressure. Therefore, the above equation becomes,

$$\omega_m^{a^2} \Phi_m + \ddot{\Phi}_m = -\frac{2c^2}{V} \sum_n \dot{q}_n \int_S \psi_m \phi_n \, \mathrm{d}s \tag{20}$$

In the fully coupled fluid–structure interaction, the pressure exerted onto the plate surface is comprised of the external loading $p_{\mathrm{ext}}(x_s, y_s, t)$ and the room-fluid loading $p(x_s, y_s, t)$. The deflection of the plate is then governed by

$$D\nabla^4 w + m_s \frac{\partial^2 w}{\partial t^2} = p_{\mathrm{ext}} - p \tag{21}$$

Note that in the uncoupled fluid–structure interaction there is no feedback of the pressure fluctuation inside the room onto the plate, which is equivalent to omitting $p$ in the above equation. This equation may be expressed in terms of summations over the acoustic and structural modes. The orthogonality properties of the structural modes are then used to reduce this partial differential equation to a finite set of ordinary differential equations as

$$\omega_n^{s^2} q_n + \ddot{q}_n = \int_S p_{\mathrm{ext}} \phi_n \, \mathrm{d}s - \sum_m a_m \int_S \phi_n \psi_m \, \mathrm{d}s \tag{22}$$

or in terms of the velocity potential

$$\omega_n^{s^2} q_n + \ddot{q}_n = \int_S p_{\mathrm{ext}} \phi_n \, \mathrm{d}s + \rho_r \sum_m \dot{\Phi}_m \int_S \phi_n \psi_m \, \mathrm{d}s \tag{23}$$

Energy dissipation in the system may be expressed by replacing the damping forces by equivalent forces that are proportional to the velocity. In this case, damping terms for the structure and the fluid will take the form $2\zeta_n^s \omega_n^s \dot{q}_n(t)$ and $2\zeta_m^a \omega_m^a \dot{\Phi}_m(t)$, where $\zeta_n^s$ and $\zeta_m^a$ are the modal damping ratios for the structure and the fluid, respectively. The formulation of the response for the damped system is essentially the same. If the structural response of the plate and acoustic response

of the room are damped, Eqs. (20) and (23) become,

$$\omega_m^{a^2}\Phi_m + 2\zeta_m^a\omega_m^a\dot{\Phi}_m + \ddot{\Phi}_m = -\frac{2c^2}{V}\sum_n \dot{q}_n \int_S \psi_m\phi_n \,\mathrm{d}s \tag{24}$$

$$\omega_n^{s^2} q_n + 2\zeta_n^s\omega_n^s\dot{q}_n + \ddot{q}_n = \int_S p_{\mathrm{ext}}\phi_n \,\mathrm{d}s + \rho_r \sum_m \dot{\Phi}_m \int_S \phi_n\psi_m \,\mathrm{d}s \tag{25}$$

The modal acoustic and structural responses may now be computed in the time domain by integrating simultaneously two coupled sets of differential equations. The numerical integration was carried out with a Newmark-$\beta$ algorithm.

## 3. Numerical results for illustrative examples

In this section, numerical results are presented for illustrative examples. The room considered is the one used for experimental validation. The room has dimensions $L_{rx} = 2.24\,\mathrm{m}$ (88 in), $L_{ry} = 2.31\,\mathrm{m}$ (91 in), and $L_{rz} = 2.59\,\mathrm{m}$ (102 in). The plaster–wood wall has dimensions $L_{sx} = 1.82\,\mathrm{m}$ (71.5 in) and $L_{sy} = 2.21\,\mathrm{m}$ (87 in), and a mass per unit area of $m_s = 25\,\mathrm{kg/m^2}$. The orthotropic constants of the wall were estimated using Eq. (6) and the first three natural frequencies of the wall obtained from modal tests. It was found that $D_x = 794$, $D_y = 1.46\times10^5$, and $D_{xy} = 1{,}8770\,\mathrm{N\,m^2}$. The modal damping ratios of the wall and the room for the first three structural and acoustic modes were determined experimentally. For the structure, it was found that $\xi_1^s = 0.038$, $\xi_2^s = 0.03$, and $\xi_3^s = 0.029$, and for the room acoustics $\xi_2^a = 0.032$, $\xi_3^a = 0.032$, and $\xi_4^a = 0.043$. Beyond the third mode, the modal damping ratios could not be accurately determined experimentally and were set as $\xi_{n>3}^s = 0.03$ and $\xi_{m>4}^a = 0.043$ as a guess. The incident wave is an N-wave in the range of that produced by the Concorde, with duration $t_d = 210\,\mathrm{ms}$, rise and fall times $t_r = t_f = 2\,\mathrm{ms}$, and maximum and minimum overpressures of $\pm100\,\mathrm{Pa}$. The time history and magnitude of the FFT of the wave are depicted in Figs. 4(a) and (b), respectively. Simulations were carried out for three orientations of the wave, at normal incidence, at $\varphi_x = \varphi_y = 45^\circ$ and $\varphi_z = 90^\circ$ (non-uniform excitation in the $x_s$-direction only), and at $\varphi_x = \varphi_y = 50^\circ$ and $\varphi_z = 65^\circ$ (non-uniform excitation in the $x_s$- and $y_s$-directions). The computation of the system response was carried out using 12 structural and 20 acoustic modes, covering a frequency range of 0–190 Hz. The modal dynamic equations were integrated from 0 to 6 s with a time step of $\Delta t = 0.5\,\mathrm{ms}$. The wall "in vacuo" natural frequencies and modal indices and the acoustic natural frequencies and modal indices for the room with hard walls are listed in Tables 1 and 2, respectively. Note that $m = 1$ in Table 2 is not truly a mode but rather corresponds to the bulk compressibility of the room and does not have a natural frequency.

Fig. 5 depicts the modal force for the first six modes and for the three wave orientations. The case of the wave at normal incidence (solid line) is considered first. As expected, the figure indicates that the loading excites only the fully symmetric modes ($n_x$ and $n_y$ odd), in the form of N-waves. These modes correspond to $n = 1$, 3, 6, and 11 in Table 1. At any instant of time, the external loading on the wall is uniform. Therefore, the modal force can only be non-zero when the mode shape has a constant displacement component. In the case of the wave with orientation $\varphi_x = \varphi_y = 45^\circ$ and $\varphi_z = 90^\circ$ (dashed line), the modal force is non-zero for all the modes that are symmetric along the $y_s$-direction (also $z$-direction), which corresponds to odd values of $n_y$ in Table 1. For the fully symmetric modes, the modal force nearly superimposes to that obtained with a wave at normal incidence but is delayed by approximately 3 ms and experiences some distortions during the rise and fall times of the N-wave overpressure. The modal structural response for the fully symmetric modes is therefore independent of the wave orientation for all practical purposes. For the modes symmetric along the $y_s$-direction only ($n_x$ even and $n_y$ odd), the modal force consists of a series of two impulses whose maxima occur at 3 and 211 ms. Fig. 6 shows the $x_s$-component of the pressure gradient integrated along the $x_s$-direction of the wall, as a function of time. Note that in this case, the $y_s$-component is zero because of the uniform excitation in the $y_s$-direction. The time history of this quantity follows the same trend as the modal force, a sequence of two impulses. Because of the wave orientation, the

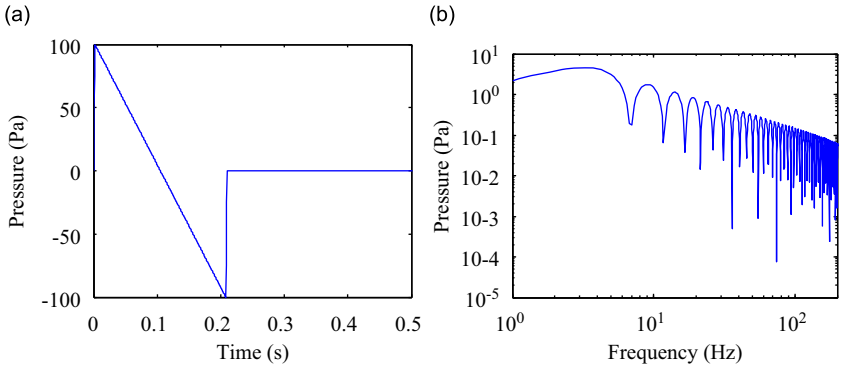


**Fig. 4.** N-wave: (a) time history and (b) magnitude of the FFT.

**Table 1**
Natural frequencies of the wall computed "in vacuo" and corresponding modal indices.

| $f_n^s$ (Hz) | $n$ | $n_x$ | $n_y$ |
|---|---|---|---|
| 28.3 | 1 | 1 | 1 |
| 40.5 | 2 | 2 | 1 |
| 57.1 | 3 | 3 | 1 |
| 78.3 | 4 | 4 | 1 |
| 102.9 | 5 | 1 | 2 |
| 104.2 | 6 | 5 | 1 |
| 116 | 7 | 2 | 2 |
| 135 | 8 | 6 | 1 |
| 136.1 | 9 | 3 | 2 |
| 162 | 10 | 4 | 2 |
| 170.8 | 11 | 7 | 1 |
| 192.8 | 12 | 5 | 2 |

**Table 2**
Acoustic natural frequencies computed for the room with hard walls and corresponding modal indices.

| $f_m^a$ (Hz) | $m$ | $m_x$ | $m_y$ | $m_z$ |
|---|---|---|---|---|
| – | 1 | 0 | 0 | 0 |
| 67.4 | 2 | 0 | 0 | 1 |
| 75.5 | 3 | 0 | 1 | 0 |
| 78.1 | 4 | 1 | 0 | 0 |
| 101.2 | 5 | 0 | 1 | 1 |
| 103.1 | 6 | 1 | 0 | 1 |
| 108.6 | 7 | 1 | 1 | 0 |
| 127.8 | 8 | 1 | 1 | 1 |
| 134.7 | 9 | 0 | 0 | 2 |
| 151 | 10 | 0 | 2 | 0 |
| 154.4 | 11 | 0 | 1 | 2 |
| 155.7 | 12 | 1 | 0 | 2 |
| 156.1 | 13 | 2 | 0 | 0 |
| 165.3 | 14 | 0 | 2 | 1 |
| 170 | 15 | 1 | 2 | 0 |
| 170.1 | 16 | 2 | 0 | 1 |
| 173 | 17 | 1 | 1 | 2 |
| 173.4 | 18 | 2 | 1 | 0 |
| 182.8 | 19 | 1 | 2 | 1 |
| 186.1 | 20 | 2 | 1 | 1 |

pressure distribution is also a function of the position on the wall surface. As a result, a pressure gradient is exerted over the wall surface provided that the slope of the shock-wave time history is non-zero. A short rise time will produce a large pressure gradient over the wall surface, and thus a larger modal force. The effect of the rise time on the response is investigated in detail in the parametric study (Section 4.2). For the wave with an orientation $\varphi_x = \varphi_y = 50^\circ$ and $\varphi_z = 65^\circ$, the fully symmetric modes are applied an N-like force, similarly to that obtained in the previous case. As expected, all the other modes ($n_x$ or $n_y$ even) are applied a force in the form of two successive impulses, as a result of a non-uniform excitation of the wall, this time in both the $x_s$- and $y_s$-directions.

Fig. 7 depicts the modal acceleration as a function of time for the first six modes and for the three wave orientations. Regardless of the wave orientation, the modal response of the wall is dominated by the first mode with some significant contribution from the third mode. For the wave at normal incidence (solid line), all the fully symmetric modes are excited, and also modes $n = 5$ and 9 as a result of the vibro-acoustic coupling. These modes are not excited when the response is computed for the uncoupled fluid–structure interaction (not plotted here). These modes are likely driven by the acoustic modes $m = 5$ and 9. However, their contribution to the response, relative to the fundamental mode, is insignificant. For a wave arriving at an angle (dashed and dotted lines), the pressure gradient exerted on the wall as a result of the wave orientation produces additional excitation to the anti-symmetric modes in the directions of the non-zero gradient components. The contribution of these modes, $n = 2$, 4, and 5 in the figure, is lower with respect to the dominant mode ($n = 1$) but not insignificant.

Fig. 8 depicts the modal pressure inside the room as a function of time for the first four modes. All the modes that are anti-symmetric along the $x$- and $z$-directions ($m_x$ and $m_z$ even) are excited. Those correspond to $m = 1$, 3, 9, 10, 11, 13, and 18 in Table 2. These modes are driven by the fully symmetric modes of the wall and thus their response is nearly insensitive

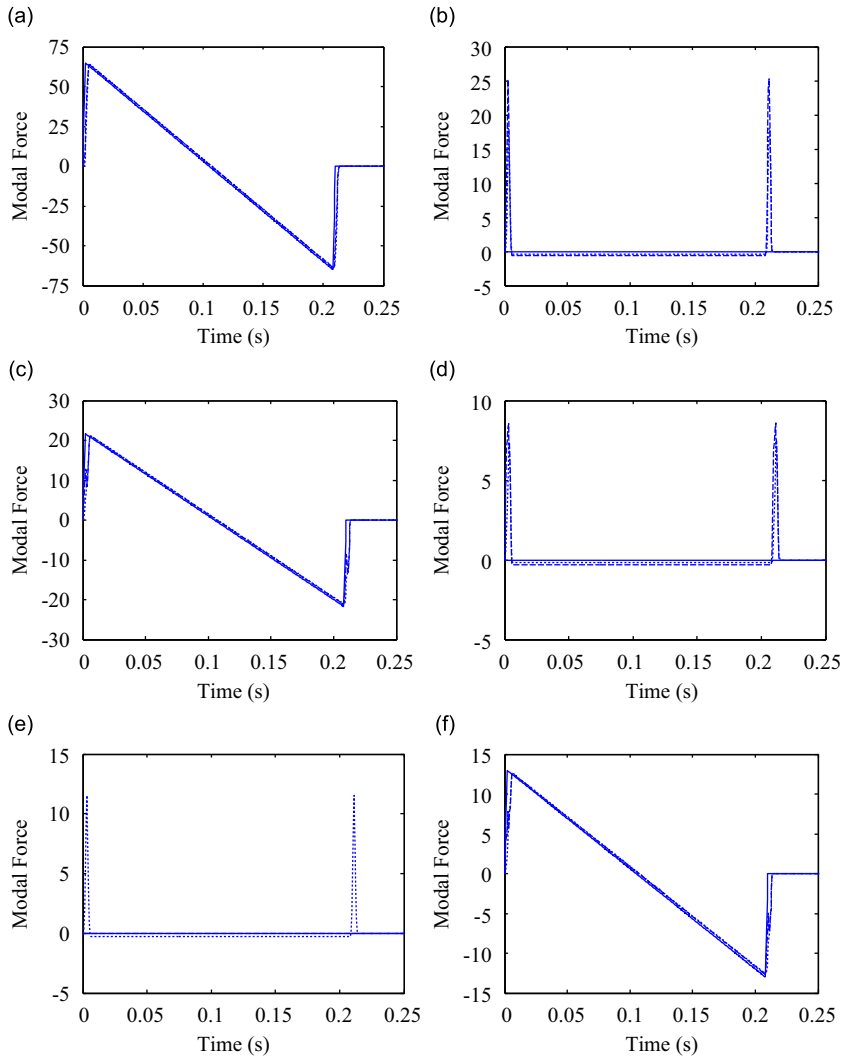


**Fig. 5.** Modal force as a function of time due to the N-wave at normal incidence (—), at $\varphi_x = \varphi_y = 45^\circ$ and $\varphi_z = 90^\circ$ (------), and at $\varphi_x = \varphi_y = 50^\circ$ and $\varphi_z = 65^\circ$ (.....), for the modes (a) $n = 1$, (b) 2, (c) 3, (d) 4, (e) 5, and (f) 6.

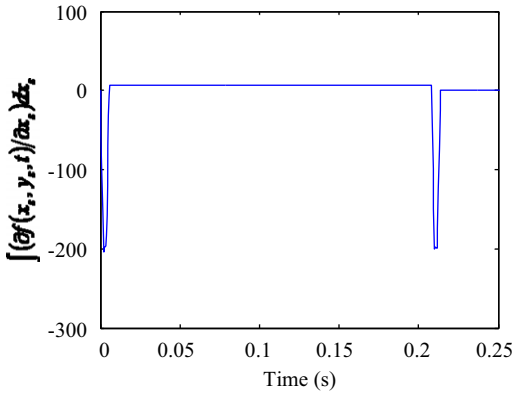


**Fig. 6.** Pressure gradient ($x_s$-component) integrated along the $x_s$-direction of the wall, as a function of time for the N-wave at $\varphi_x = \varphi_y = 45^\circ$ and $\varphi_z = 90^\circ$.

to the wave orientation. Note that the acoustic modes may be excited for any $m_y$ since the wall deflection is assumed to be normal to the wall surface, in the $y$-direction. The modal acoustic response is dominated by the bulk-compressibility of the cavity ($m = 1$), whose time history is comparable to the superposition of an N-wave and a damped sine wave at 28.3 Hz,

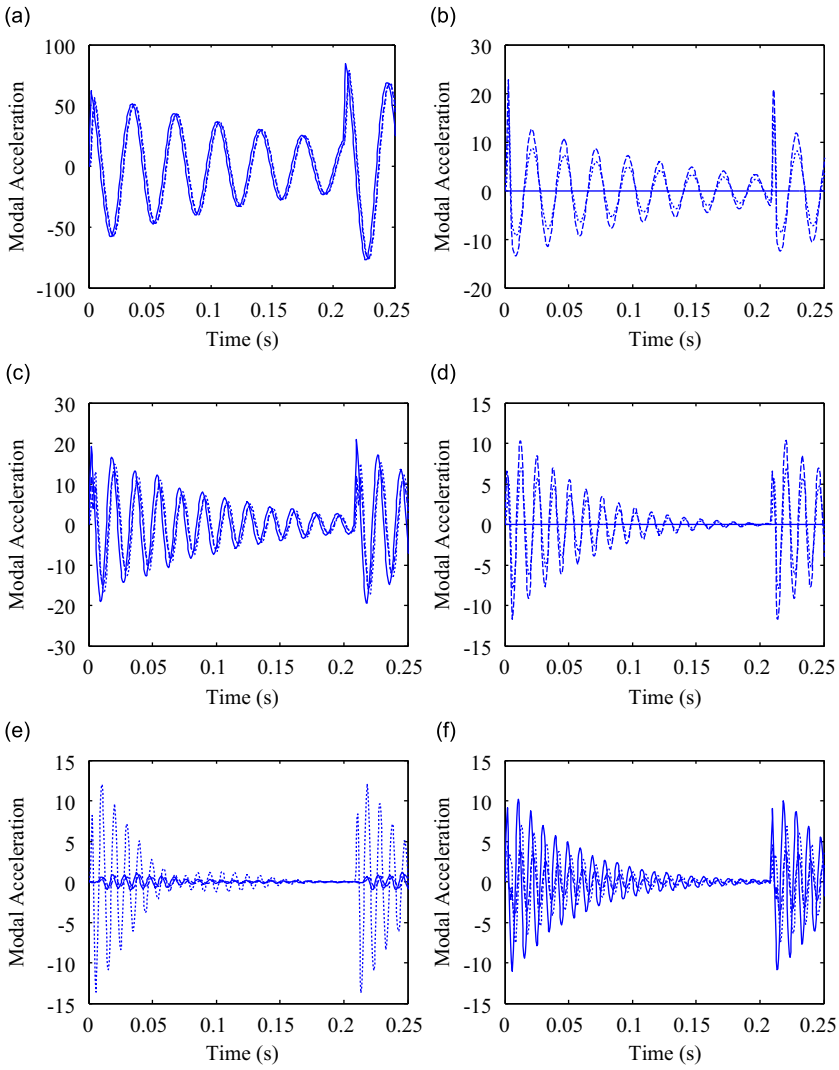


**Fig. 7.** Modal acceleration of the wall as a function of time due to the N-wave at normal incidence (———), at $\varphi_x = \varphi_y = 45^\circ$ and $\varphi_z = 90^\circ$ (------), and at $\varphi_x = \varphi_y = 50^\circ$ and $\varphi_z = 65^\circ$ (.....), for the modes (a) $n = 1$, (b) 2, (c) 3, (d) 4, (e) 5, and (f) 6.

that of the first structural mode. The third acoustic mode is the only other mode contributing in a significant manner to the acoustic response.

Fig. 9 shows the time histories (left) and magnitudes of the FFT (right) of the accelerations at the center of the wall and at $x_s = 0.41$ m and $y_s = 0.5$ m (near a corner of the wall), for the three wave orientations. At the center of the wall, because of symmetry, only the fully symmetric modes contribute to the response. The first consequence of this is a drop of magnitude observed in the spectrum between 60 and 100 Hz. The second consequence is the insensitivity of the structural response to the wave orientation. Near a corner of the wall, the effect of the wave orientation is more visible as the anti-symmetric modes also contribute to the response. The structural modes excited by the pressure gradient over the wall surface as the wave arrives at an angle are responsible for the increase in magnitude of the acceleration in the frequency ranges 40–50 Hz, and 100–120 Hz. However, the response remains largely dominated by the fundamental mode. Therefore, the structural response is virtually independent of the wave orientation.

Acoustic pressures computed at the center of the wall surface and at the center of the room for the three wave orientations are shown in Fig. 10. It is clear that the dominant part of the acoustic response spectrum is due to the first structural mode at 28.3 Hz. The first acoustic resonance takes place at 67 Hz and thus the acoustic bulk compressibility of the room, $m = 1$, is the only term contributing to the response below 67 Hz. The higher frequency content provided by the third acoustic mode is observed at the center of the wall surface only. Because of symmetry, the third mode, which is anti-symmetric in the y-direction ($m_y$ odd), does not contribute to the response at the center of the room. The acoustic response

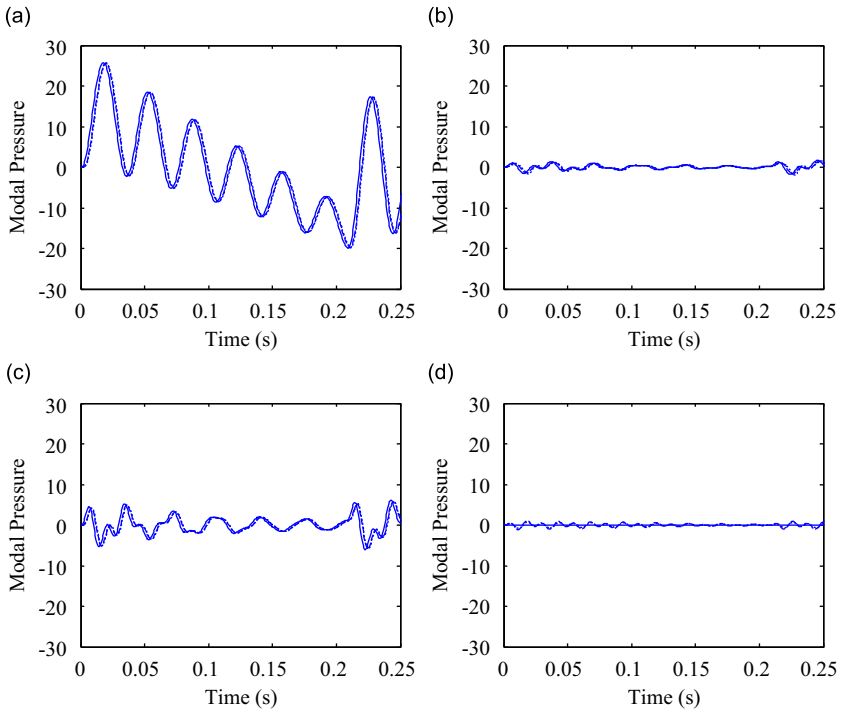


**Fig. 8.** Modal pressure as a function of time due to the N-wave at normal incidence (———), at $\varphi_x = \varphi_y = 45^\circ$ and $\varphi_z = 90^\circ$ (------), and at $\varphi_x = \varphi_y = 50^\circ$ and $\varphi_z = 65^\circ$ (.....), for the modes: (a) $m = 1$, (b) 2, (c) 3, and (d) 4.

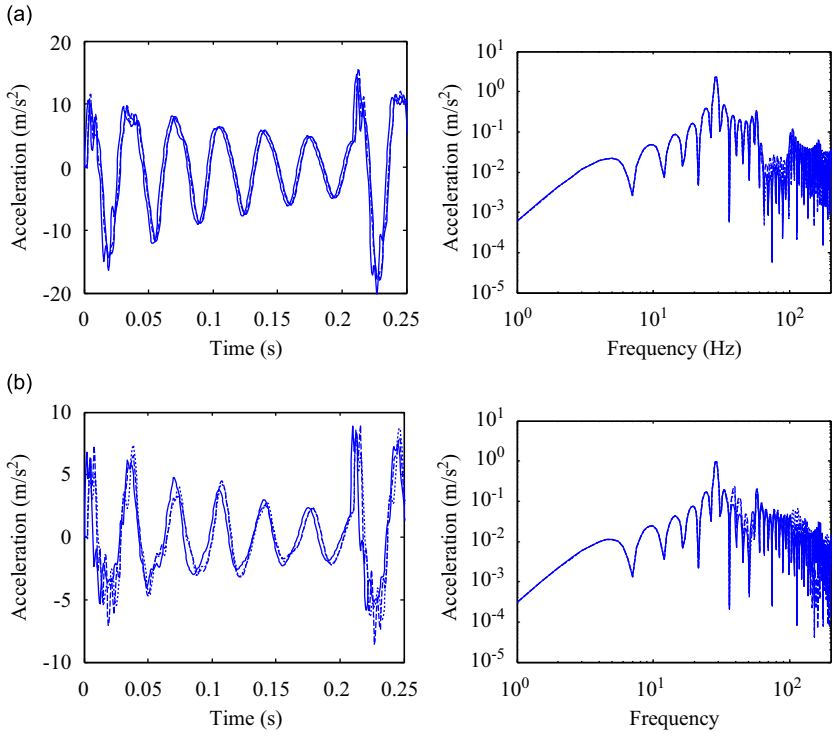


**Fig. 9.** Accelerations of the wall, time histories (left) and magnitudes of the FFT (right): (a) at the center of the wall and (b) at $x_s = 0.41$ m and $y_s = 0.5$ m.

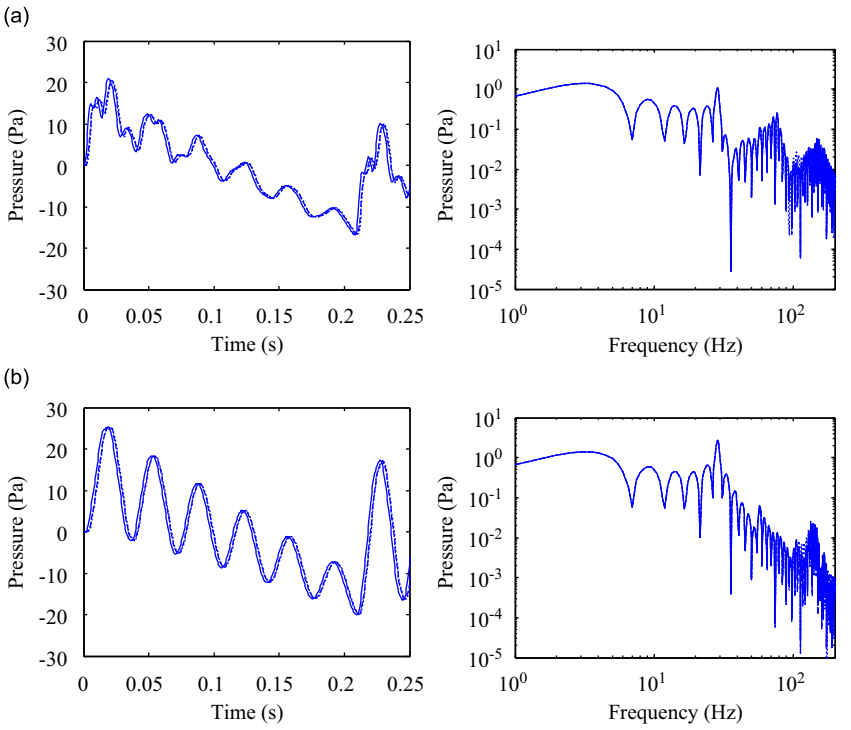


**Fig. 10.** Pressures inside the room, time histories (left) and magnitudes of the FFT (right): (a) close to the center of the wall surface and (b) at the center of the room.

at both positions in the room is dominated by the bulk compressibility and thus, like the wall response, is from the practical point of view independent of the wave orientation.

## 4. Parametric study

A parametric study was conducted to assess the effects of the incident wave parameters and effects of the wall and room dimensions on the system response. It was shown in the previous section that the orientation of the wave with respect to the structure has virtually no effect on the system response. Therefore, all calculations carried out in this section are for shock waves arriving onto the wall at normal incidence.

### *4.1. Effect of N-wave duration*

The wave considered in this subsection is an N-wave with maximum and minimum overpressures of $\pm 100$ Pa, rise and fall times $t_r = t_f = 2$ ms, and a duration that is varied from $t_d = 10$–$300$ ms in 2-ms increments. The room and wall have the same dimensions as in the previous section, which are $L_{rx} = 2.24$ m, $L_{ry} = 2.31$ m, $L_{rz} = 2.59$ m, $L_{sx} = 1.82$ m, and $L_{sy} = 2.21$ m. Calculations were also carried out for the same geometry but with an increased room depth, $L_{ry} = 6.17$ m, such that the natural frequency of the third acoustic mode, (0,1,0) mode, matches that of the first structural mode, (1,1) mode.

To make meaningful comparisons between the responses, it is necessary to define some dimensionless parameters. The peak amplitude of the acceleration times $m_s$ at a given point on the wall surface, $\ddot{w}^{\max}$, compared to the shock wave overpressure, $p_{sw}^{\max}$, defines the peak amplitude ratio $R_a = m_s \ddot{w}^{\max}/p_{sw}^{\max}$. Similarly, the largest pressure at a given point inside the room, $p^{\max}$, compared to the shock wave overpressure defines the peak amplitude ratio $R_p = p^{\max}/p_{sw}^{\max}$. It was shown in the previous section that the system response is dominated by the first structural mode. Therefore, the boom duration is normalized by the fundamental mode period, i.e. $T_d^s = t_d f_1^s$ where $f_1^s$ is the natural frequency of the first structural mode.

Fig. 11 shows the amplitude ratio of the acceleration at the center of the wall as a function of the normalized boom duration. For the room with a depth of 2.31 m (solid curve), the amplitude ratio is maximum for $T_d^s = 0.85$ and then reaches local maxima at integer multiples of $T_d^s$. This result is in good agreement with the fact that the structural response is indeed dominated by the fundamental mode. For the room with a depth $L_{ry} = 6.17$ m (dashed line), $R_a$ does not exactly follow this

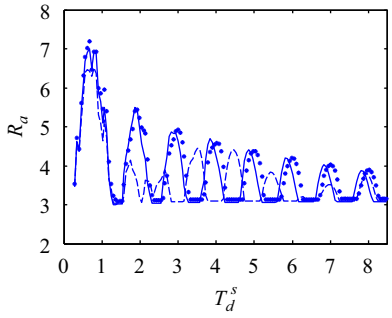


**Fig. 11.** Amplitude ratio of the acceleration $R_a$ at the center of the wall as a function of the structural period ratio $T_d^s$ ($t_r = 2$ ms). Fully coupled fluid–structure interaction, $L_{ry} = 2.31$ m (———) and $L_{ry} = 6.17$ m (------). Uncoupled fluid–structure interaction, $L_{ry} = 2.31$ m ( × ) and $L_{ry} = 6.17$ m (+).

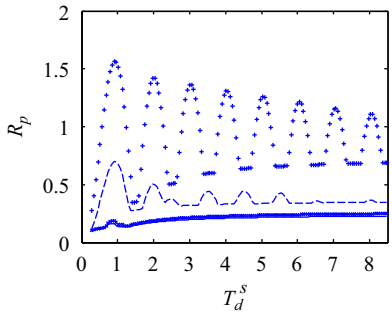


**Fig. 12.** Amplitude ratio of the pressure $R_p$ close to the center of the wall surface as a function of the period ratio $T_d^s$ ($t_r = 2$ ms). Fully coupled fluid–structure interaction, $L_{ry} = 2.31$ m (———) and $L_{ry} = 6.17$ m (------). Uncoupled fluid–structure interaction, $L_{ry} = 2.31$ m ( × ) and $L_{ry} = 6.17$ m (+).

trend. It exhibits a slightly lower amplitude as a result of the vibro-acoustic coupling that occurs between the first structural and third acoustic modes. This fact can be verified by omitting the term corresponding to the room acoustic pressure in the dynamic equation of the wall, i.e. artificially removing vibro-acoustic coupling when computing the system response. In the absence of coupling, the variation of $R_a$ with $T_d^s$ is the same for $L_{ry} = 2.31$ m (" × " markers) and $L_{ry} = 6.17$ m ("+" markers).

Fig. 12 shows the amplitude ratio of the pressure close to the center of the wall surface as a function of the normalized boom duration. For the room with a depth of 2.31 m (solid line), the amplitude ratio only exhibits one local maximum value, when $T_d^s = 0.85$. A similar result was obtained by Wahba et al. [15] in the study of the transmission of sonic booms inside a room with an open window. The fact that no peak was observed for integer values of $T_d^s$ higher than 1 was demonstrated to be caused by damping. As the undamped problem was solved, these peaks could then be observed. For the room with a depth of 6.17 m (dashed line), the asymptotic value $R_p$ tends to, is larger than that for a room depth of 2.31 m and local maxima are observed for values of $T_d^s$ larger than unity. These maxima may now be observed because damping decreases as the volume of the room increases. In the absence of vibro-acoustic coupling, only the response of the room with a depth of 6.17 m is changed. The amplitude ratio exhibits then a much larger value than for the fully coupled system and local maxima when $T_d^s$ is an integer. This result also suggests the need to consider the fluid–structure interaction fully coupled for the solution to be truly representative.

### 4.2. Effect of N-wave rise time

To study the effect of the N-wave rise time, the system response was computed for N-waves with maximum and minimum overpressures of $\pm 100$ Pa, period ratios $T_d^s = 1$ ($t_d = 36$ ms), 3 ($t_d = 108$ ms), 5 ($t_d = 180$ ms), and 7 ($t_d = 252$ ms), and rise and fall times that are varied from $t_r = t_f = 0$ to $t_d/4$. To assess the effect on the system response of smoothing out the peak of the N-wave overpressure, simulations were also carried out for the excitation being one period of a sine wave of period $t_d$ with maximum and minimum overpressures of $\pm 100$ Pa. The room and wall have dimensions $L_{rx} = 2.24$ m, $L_{ry} = 2.31$ m, $L_{rz} = 2.59$ m, $L_{sx} = 1.82$ m, and $L_{sy} = 2.21$ m.

It is interesting to examine the frequency content of an incident wave regardless of the wave duration or amplitude. For this purpose, the weighted energy $E$ at a frequency $f$ is defined as the amount of power contained in the frequency band 0–$f$ relative to the total power of the incident wave. The weighted energy was computed as a function of the normalized frequency $F_d = f \times t_d$ and is plotted in Fig. 13 for a perfect N-wave (solid line) and N-wave with rise time $t_r = t_d/4$ (dashed line). There is critical frequency, $F_d^c = 1.2$, below which the spectral density of the perfect N-wave is larger than that of an N-wave with rise time $t_d/4$ and above which it is smaller. This means that N-waves with longer rise times contain more energy in their low frequency components than those with smaller rise times. This result suggests that the amplitude of the structural response due to an N-wave with rise time $t_d/4$ will be larger than that due to a perfect N-wave around resonance ($T_d^s = 1$), and smaller above resonance.

Figs. 14 and 15 show the amplitude ratios of the acceleration at the center of the wall and pressure close to the center of the wall surface as a function of the normalized rise time defined as $T_r = t_r/t_d$. In the figures, the hollow circles, squares, triangles, and diamonds correspond to N-waves with $T_d^s = 1$, 3, 5, and 7, respectively. The solid circles, squares, triangles,

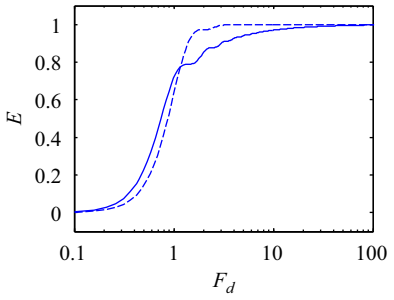


**Fig. 13.** Weighted energy $E$ as a function of normalized frequency $F_d$. N-waves with rise times $t_r = 0$ (———) and $t_d/4$ (------).

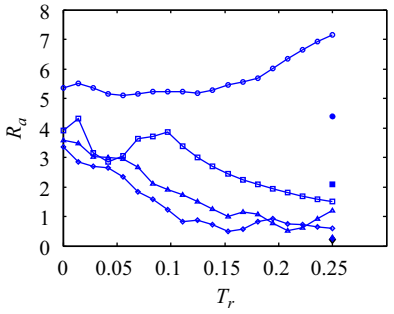


**Fig. 14.** Amplitude ratio of the acceleration $R_a$ at the center of the wall as a function of the normalized rise time $T_r$. Excitation: N-wave with $T_d^s = 1$ (◦), 3 (□), 5 (Δ), and 7 (◇); one period of a sine wave with $T_d^s = 1$ (●), 3 (■), 5 (▲), and 7 (♦).

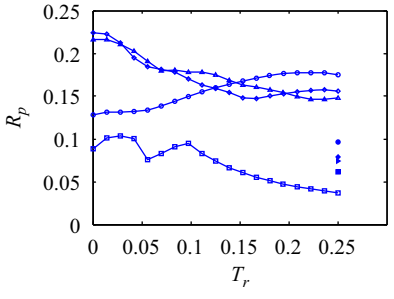


**Fig. 15.** Amplitude ratio of the pressure $R_p$ close to the center of the wall surface as a function of the normalized rise time $T_r$. Excitation: N-wave with $T_d^s = 1$ (◦), 3 (□), 5 (Δ), and 7 (◇); one period of a sine wave with $T_d^s = 1$ (●), 3 (■), 5 (▲), and 7 (♦).

and diamonds correspond to one period of a sine wave with $T_d^s = 1$, 3, 5, and 7, respectively. The amplitudes of the acceleration and pressure increase with the rise time when the boom duration is the same as the natural period of the first structural mode, i.e. $T_d^s = 1$ (hollow circles) which is analogous to driving the structure at resonance. On the other hand, it decreases when $T_d^s$ is much larger than unity, for instance $T_d^s = 5$ (hollow triangles) and $T_d^s = 7$ (hollow diamonds). In the transition between these two cases, e.g. $T_d^s = 3$ (hollow squares), the amplitudes of the acceleration and pressure decrease with $T_r$ for part of the $T_r$ range only. For all cases except $T_d^s = 3$, the system response due to a one-period sine wave is much smaller than that due to an N-wave with rise time $t_d/4$. The fact that for $T_d^s = 3$ the amplitudes do not follow this trend is because at $f = f_1^s$, the spectrum of the N-wave with rise time $t_d/4$ exhibits a minimum of magnitude whereas that of the sine wave does not.

### 4.3. Effects of wall and room dimensions

Studying the system response at fixed boom characteristics and varying room dimensions is the inverse problem of that solved in Section 4.1. The incident waves are N-waves with durations of 36 and 210 ms, and a rise time of 2 ms. The fundamental frequency of the wall is varied from $f_1^s = 10$ to 80 Hz in 2 Hz increments. With an aspect ratio of 1.25 such that, $L_{sy} = 1.25 \times L_{sx}$, this is equivalent to varying $L_{sx}$ from 3 to 1.1 m. For each wall dimension, the natural frequency of the third acoustic mode, (0,1,0) modes, is varied from $f_3^a = 20$ to 80 in 2 Hz increments, which is equivalent to decreasing $L_{ry}$ from 8.6 to 2.1 m. The other two room lengths were set equal to those of the wall. The frequencies of the third acoustic modes are normalized and the acoustic period ratio is defined as $T_d^a = t_d f_3^a$.

Variation of the amplitude ratio of the acceleration at the center of the wall with the structural and acoustic period ratios is shown in Figs. 16(a) and (b) for N-waves with durations of 36 and 210 ms, respectively. At a given acoustic period ratio, the amplitude of the acceleration is the largest when $T_d^s = 0.85$ and then reaches local maxima approximately when $T_d^s$ has an integer value, which is in good agreement with the results obtained in Section 4.1. At a fixed integer value of $T_d^s$, the amplitude of the acceleration oscillates with $T_d^a$ as a result of the fluid–structure coupling.

Variation of the amplitude ratio of the pressure close to the center of the wall surface with the structural and acoustic period ratios is shown in Fig. 17. The amplitude of the pressure increases with $T_d^a$ (or with the room depth). The figure also suggests that maxima of amplitudes are reaches when $T_d^s$ and $T_d^a$ are equal the same integer value, the largest value being reached when $T_d^s = T_d^a = 1$.

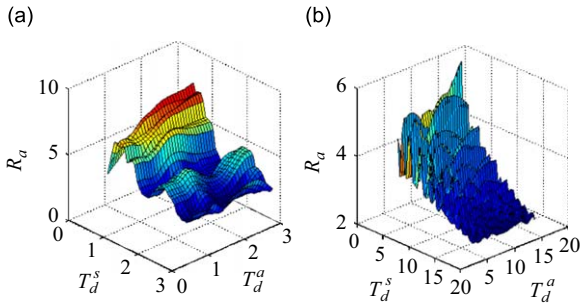


**Fig. 16.** Amplitude ratio of the acceleration $R_a$ at the center of the wall as a function of the structural and acoustic period ratios $T_d^s$ and $T_d^a$: (a) $t_d = 36$ ms and (b) $t_d = 210$ ms.

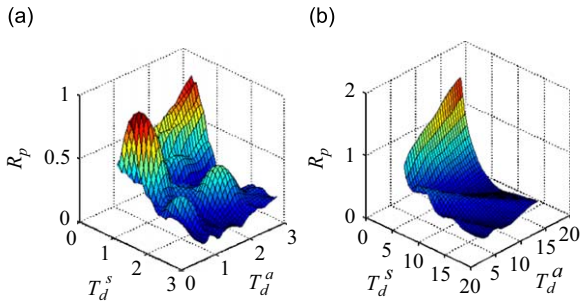


**Fig. 17.** Amplitude ratio of the pressure $R_p$ close to the center of the wall surface as a function of the structural and acoustic period ratios $T_d^s$ and $T_d^a$: (a) $t_d = 36$ ms and (b) $t_d = 210$ ms.

## 5. Experimental validation of the numerical model

### 5.1. Experimental setup

Fig. 18(a) shows the test structure consisting of a plaster–wood wall mounted in the rectangular opening of a cinderblock room. The plaster wood wall was built using standard construction techniques [16]. The wall frame shown in Fig. 18(b) was made of $3.8 \times 8.9$-cm ($1.5 \times 3.5$-in) studs spaced 30 and 40 cm (12 and 16 in) apart. The frame was sandwiched between wood panel oriented strand boards (OSB) and plaster boards that were fastened to the studs to form the outside and inside wall surfaces, respectively. The OSB and plaster boards had a thickness of 1.27 cm (1/2 in) and masses per unit area of 7.6 and 8.6 kg/m$^2$, respectively. Cavities in the wall were filled in with standards R-13 insulation. The finished wall was 2.21-m (87-in) long, 1.82-m (71.5-in) wide, and 11.4-cm (4.5-in) thick, with a mass per unit area of 25 kg/m$^2$. The cell had a width of 2.23 m (88 in), a height of 2.6 m (102 in), and a depth of 2.3 m (91 in). A wood frame was secured into the opening of the cinderblock cell to mount the wall. The wall was fastened to the frame by its internal studs using mounting brackets. Self-expanding foam was inserted into the gaps between the wall and the room to minimize leakage.

A speaker built in-house was used to produce the external pressure loading on the wall. The speaker was made of a Tsuzureko 63.5-cm (25-in) subwoofer driver and a sealed cubic enclosure of 80 cm (31.5 in). The speaker was placed in front of the wall at 2 m from the center. N-waves with durations ranging from 10 to 33.6 ms were played. The input signal had to be pre-distorted to account for the dynamics of the speaker–amplifier system and yield the desired output waveform. The wave superposition technique was used for this purpose [8]. As an example of the method, Fig. 19(a) shows the desired

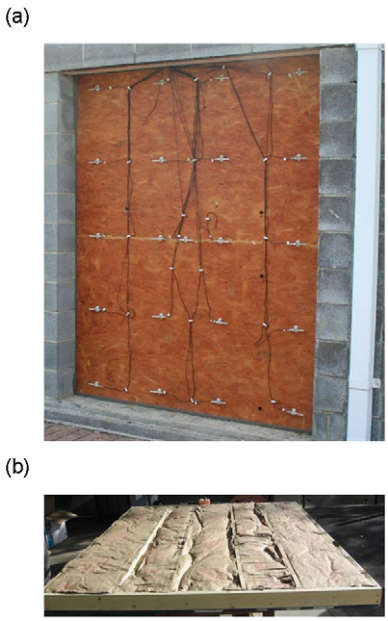


**Fig. 18.** (a) Plaster–wood wall instrumented with microphones and installed in the cinderblock room and (b) wall frame with insulation.

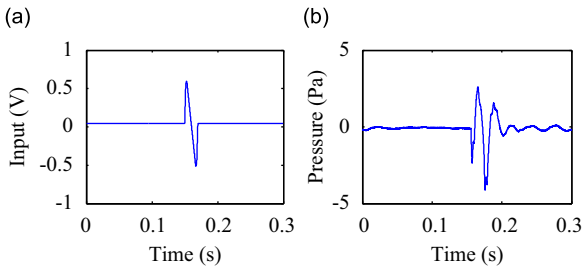


**Fig. 19.** Measured (a) input and (b) output waveforms before pre-distorting the input signal.

output waveform. This signal is input to the speaker and the response of a microphone on the structure recorded as shown in Fig. 19(b). These two time histories are then used to estimate how the input signal needs to be modified to account for the speaker dynamics and the presence of the structure. Fig. 20(a) shows the new signal that needs to be fed to the speaker after applying this method. The resulting response at the microphone is then shown in Fig. 20(b) that matches the original desired signal in Fig. 19(a) quite well.

The external pressure loading was monitored with an array of 21 microphones mounted to the outside of the wall, following the pattern shown in Fig. 21. In addition, three microphones were used to monitor the interior acoustics. These were positioned close to the center of the wall surface, center of the room, and in a corner of the room. The microphones were $\frac{1}{4}$-in Panasonic WM-60AY Electret models with a standard instrumentation amplifier conditioning circuit. An array of

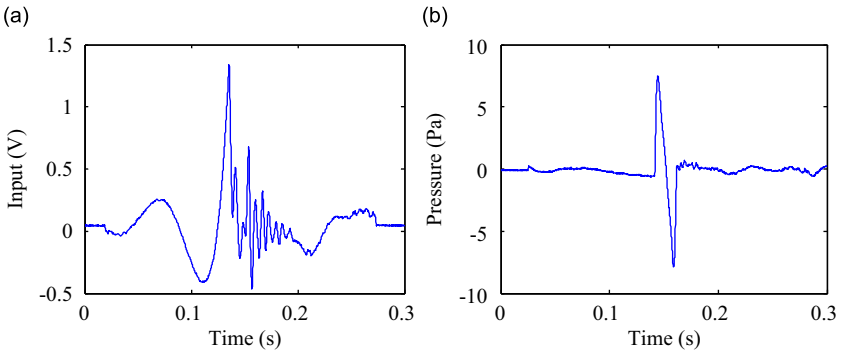


**Fig. 20.** Measured (a) input and (b) output waveforms after pre-distorting the input signal.

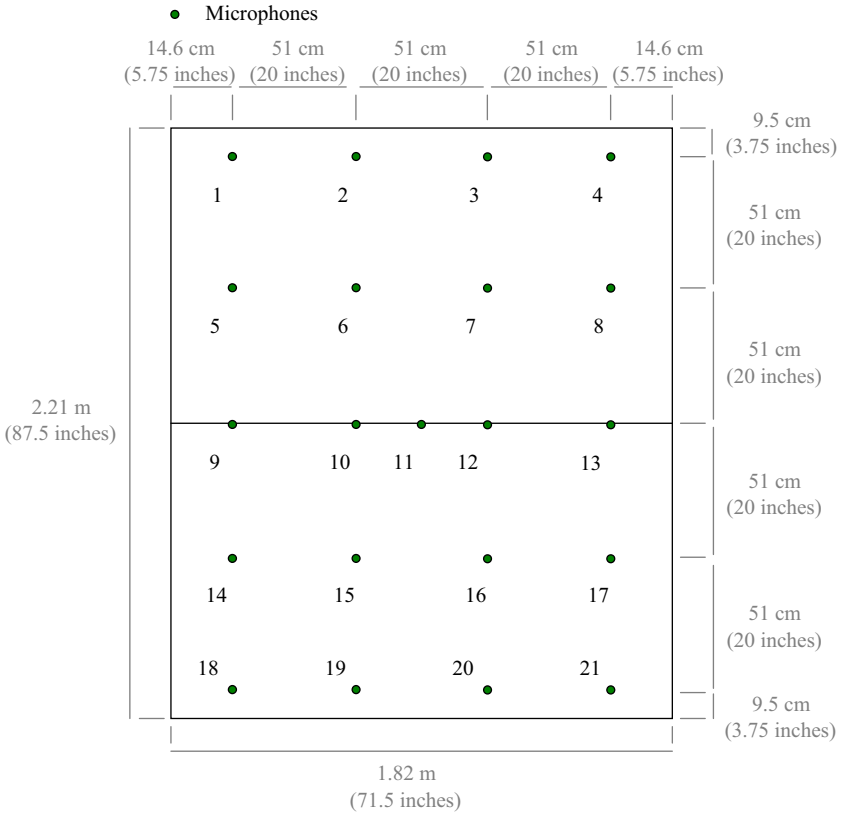


**Fig. 21.** Locations of microphones mounted to the outside wall surface.

36 accelerometers was mounted to the inside of the wall (on the plaster) to monitor the wall vibration, following the pattern shown in Fig. 22. The accelerometers were PCB model 330A calibrated in house. The microphone and accelerometer signals were acquired simultaneously with a sampling frequency of 12.8 kHz.

### 5.2. Experimental modal analysis

Modal testing was performed on the wall installed in test cell to determine the modal parameters needed for the numerical predictions. Fig. 23 is a picture of the experimental setup. A Ling Dynamic Systems (LDS) model 408 shaker hanging from an aluminum stand and attached to the structure with a stinger was used to excite the wall. The accelerometer array mentioned previously recorded the resulting response and a PCB 208A03 force transducer was used to measure the input force. The shaker was driven with white noise and data was collected at 6400 Hz for several input configurations. The wall was excited at three different positions along the wall studs with two different levels of excitation at each position. Two of these positions were symmetric with respect to the center of the wall, to check for reciprocity. The third position, near a corner of the wall, was selected such that all the modes were excited. Testing two excitation levels showed that the structure behaved linearly.

Following Ewins [17], the measured transfer functions (FRFs) between the accelerometers and the force transducer were then calculated and used to extract the modal parameters. Coherence between the accelerometers and force transducer signals was also calculated to assess the quality of the measured FRFs. A sample FRF is plotted in Fig. 24 and its associated coherence in Fig. 25. These figures indicate that resonance peaks may be detected and the coherence is reasonable for experimental data in the frequency ranges around the resonances, so modal analysis was carried out. Modal damping ratios were estimated using the half-power method. Modal parameters of the wall for the first three modes are listed in Table 3. Beyond the third mode, the modal parameters could not be accurately determined. Mode shapes were then computed using the values of the complex FRFs at the natural frequencies listed in Table 3. The first three mode shapes of the wall are shown in Fig. 26. For the plots, a finer grid than that used to position the accelerometers was generated by interpolation. The figure indicates that the modes are similar to those of a simply supported orthotropic plate with a larger stiffness in the $y$- than in the $x$-direction. Based on these results, the wall was modeled as a uniform orthotropic plate with simply supported boundary conditions. Neglecting shear effects, the dynamic properties of the wall can be defined in term of the mass density and the three orthotropic bending stiffness constants, i.e. $D_x$, $D_y$, and $D_{xy}$. The mass density is determined from

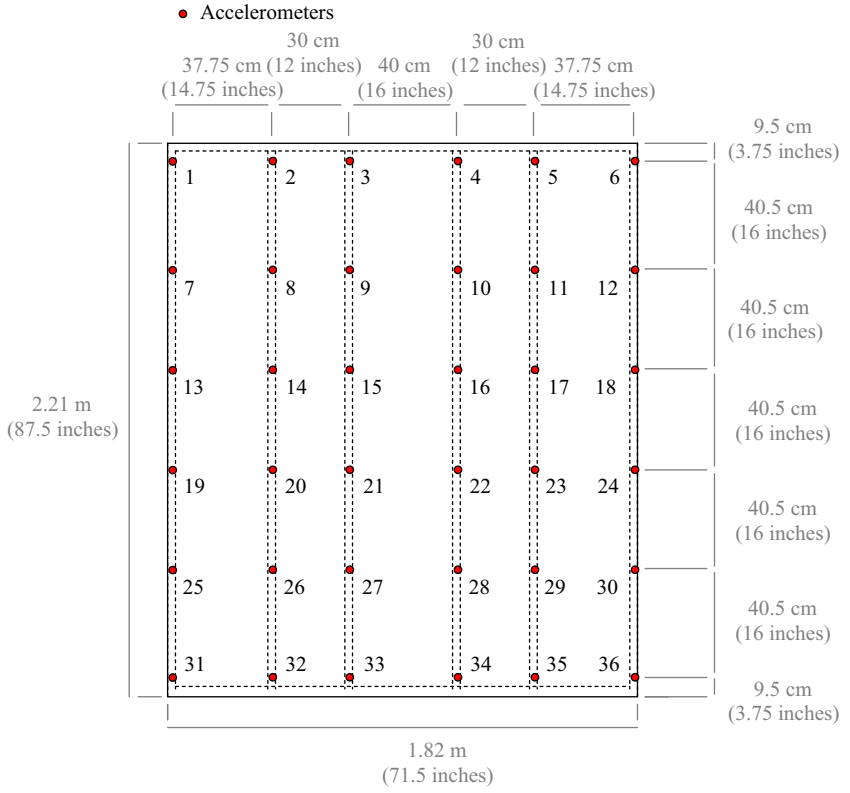


**Fig. 22.** Locations of accelerometers mounted to the inside wall surface.

**Fig. 23.** Experimental setup of the modal test.

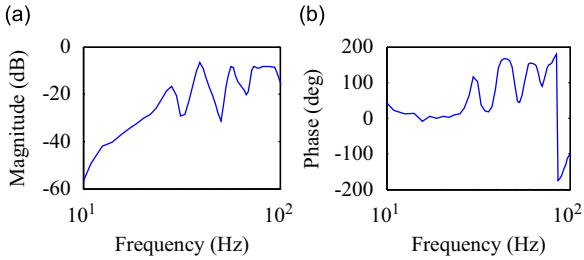


**Fig. 24.** Measured FRF from accelerometer 11: (a) magnitude and (b) phase.

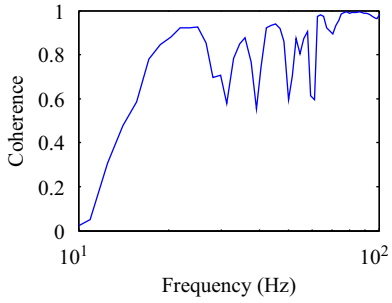


**Fig. 25.** Measured coherence from accelerometer 11.

**Table 3**
First three natural frequencies and modal damping ratios of the wall determined experimentally.

| $n$ | $f_n^s$ (Hz) | $\xi_n^s$ |
|---|---|---|
| 1 | 28.3 | 0.038 |
| 2 | 40.5 | 0.03 |
| 3 | 57.1 | 0.029 |

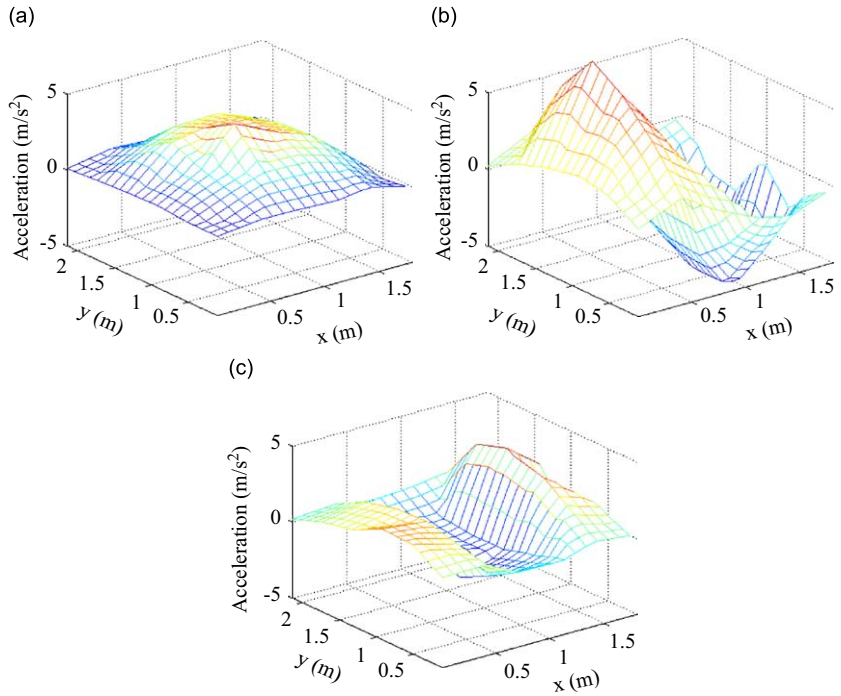


**Fig. 26.** First three modes shapes of the plain wall: (a) mode 1 at $f_1 = 28.3$ Hz, (b) mode 2 at $f_2 = 40.5$ Hz, and (c) mode 3 at $f_3 = 57.1$ Hz.

**Table 4**
First three acoustic natural frequencies and modal damping ratios of the room determined experimentally.

| $m$ | $f_m^a$ (Hz) | $\xi_m^a$ |
|---|---|---|
| 2 | 64 | 0.032 |
| 3 | 75 | 0.032 |
| 4 | 81 | 0.043 |

the total mass of the wall. The orthotropic constants may be determined knowing the first three natural frequencies of the wall reported in Table 1 and using Eq. (6).

To estimate the modal acoustic damping ratios and natural frequencies, a speaker playing white noise was placed in a corner of the room. The pressure fluctuation inside the room was recorded with the three inside microphones described above. The pressure spectra along with the half power method were used to estimate the natural frequencies and modal damping ratios for the first three acoustic modes. Those are listed in Table 4. The first three resonances in the room were found at 64, 75, and 81 Hz, which lines up closely to the natural frequencies of a rectangular room with hard walls that are reported in Table 2.

### 5.3. Comparison of numerical predictions to the experimental data

In this section, the predicted vibro-acoustic response of the structure is compared to experimental data. The analysis of the results is carried out for two sonic boom durations, 20 and 33.6 ms. The latter wave duration is close to the period of the fundamental structural mode.

Attempting to generate a sonic boom with a speaker has shortcomings, due to the wide spectrum of frequency content of an N-wave. The peaks of the input N-wave were rounded to avoid a high frequency content that the speaker would not reproduce. Microphone 11 (center of the wall) was used to determine the proper input signal to drive the speaker-amplifier system to generate the booms at this microphone location.

Pressure time histories recorded by microphones 1, 11, 13, and 18 on the outside wall surface due to N-waves with durations of 20 and 33.6 ms are shown in Fig. 27. The pressure spectra for the two wave durations are shown in Fig. 28. Pressure time histories recorded right in front of the speaker, microphone 11, indicate that the waveform is almost a perfect weak sonic boom (the desired signal) for both wave durations. One fundamental difference between the two cases presented is the peak of pressure produced after the shockwave with a duration 33.6 ms. This duration corresponds to

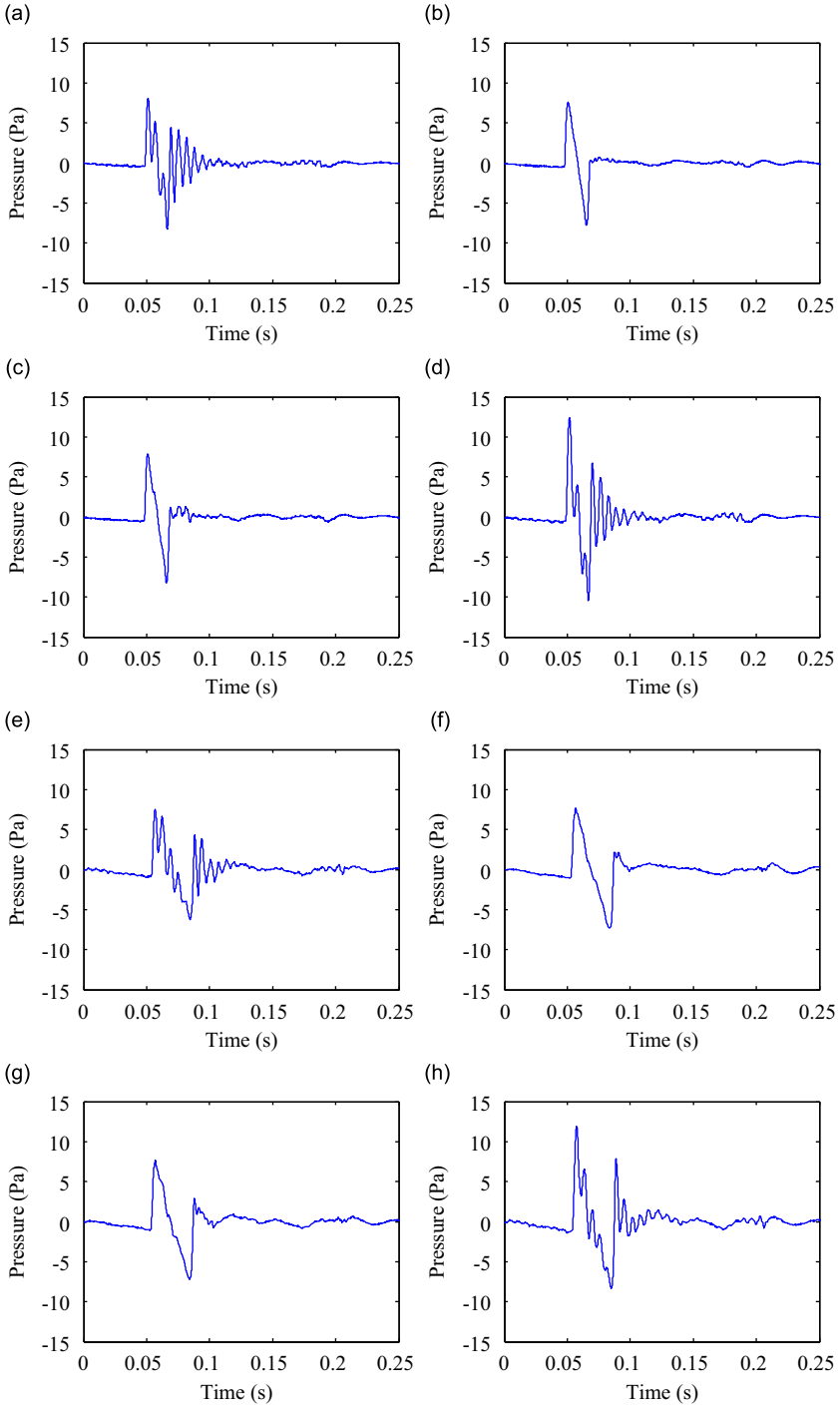


**Fig. 27.** Pressures on the outside wall surface as a function of time, for a sonic boom with a duration of 20 ms recorded by microphones (a) 1, (b) 11, (c) 13, and (d) 18, and for a sonic boom with a duration of 33.6 ms recorded by microphones (e) 1, (f) 11, (g) 13, and (h) 18.

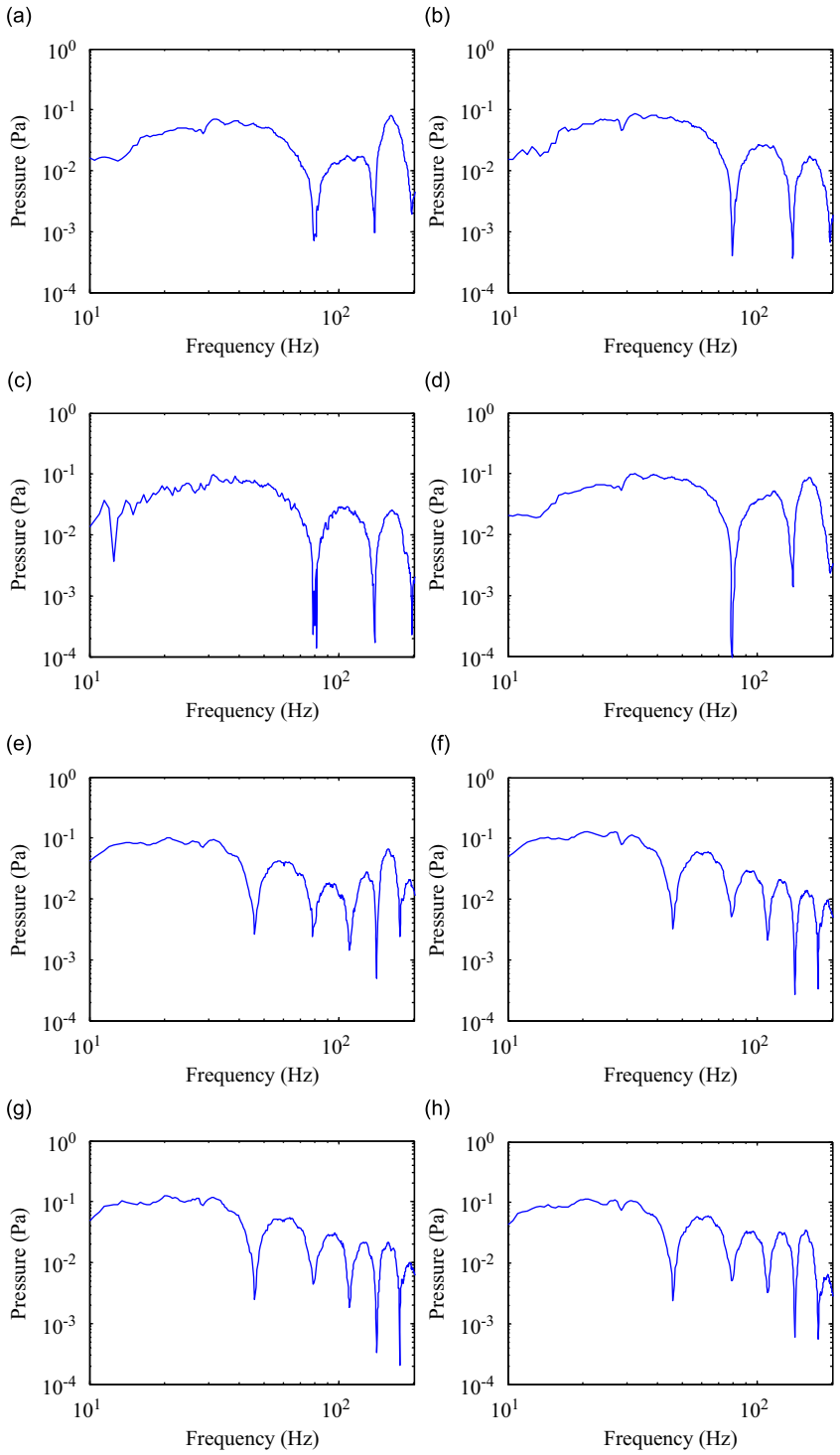


**Fig. 28.** Magnitudes of the FFT of the pressures on the outside wall surface, for a sonic boom with a duration of 20 ms recorded by microphones (a) 1, (b) 11, (c) 13, and (d) 18, and for a sonic boom with a duration of 33.6 ms recorded by microphones (e) 1, (f) 11, (g) 13, and (h) 18.

about 28 Hz, which is below the cutoff frequency of the speaker/enclosure system (36 Hz). As a result, the speaker is unable to accurately reproduce the low frequency content. At other locations along the mid-height of the wall (e.g. microphone 13), the waveform remains mostly the same. However, away from the mid-height of the wall (e.g. microphones 1 and 18),

the signal is distorted and different from the boom shape observed (and sought) with microphone 11. In the frequency domain, this distortion corresponds to a higher magnitude of the pressure near 162 Hz, as may be seen in Figs. 28(a), (d), (e), and (h). The reason for the signal distortion is the result of ground reflections. The incident wave on the wall consists of the direct wave and the ground-reflected wave. There is a small delay of the reflected wave as compared to the direct one. The interference between these two waves away from the center microphone leads to the high frequency content distortion observed. A more uniform wall excitation can be achieved by generating the shock waves with two speakers at two different heights. The signals of several wall mounted microphones would then be used to determine the proper input signal to feed to the speakers. This method is currently under investigation.

From the 21 microphones signals, a grid of $31 \times 31$ points was created over the wall surface by interpolation to describe the pressure loading on the surface. This experimental set of data was then used as an input to the model for validation purposes. Since the input data consists of the pressure recorded by the microphones directly over the wall surface, it also accounts for the diffraction of the incident wave over the edges and corners of the cinderblock room as well as the radiated field.

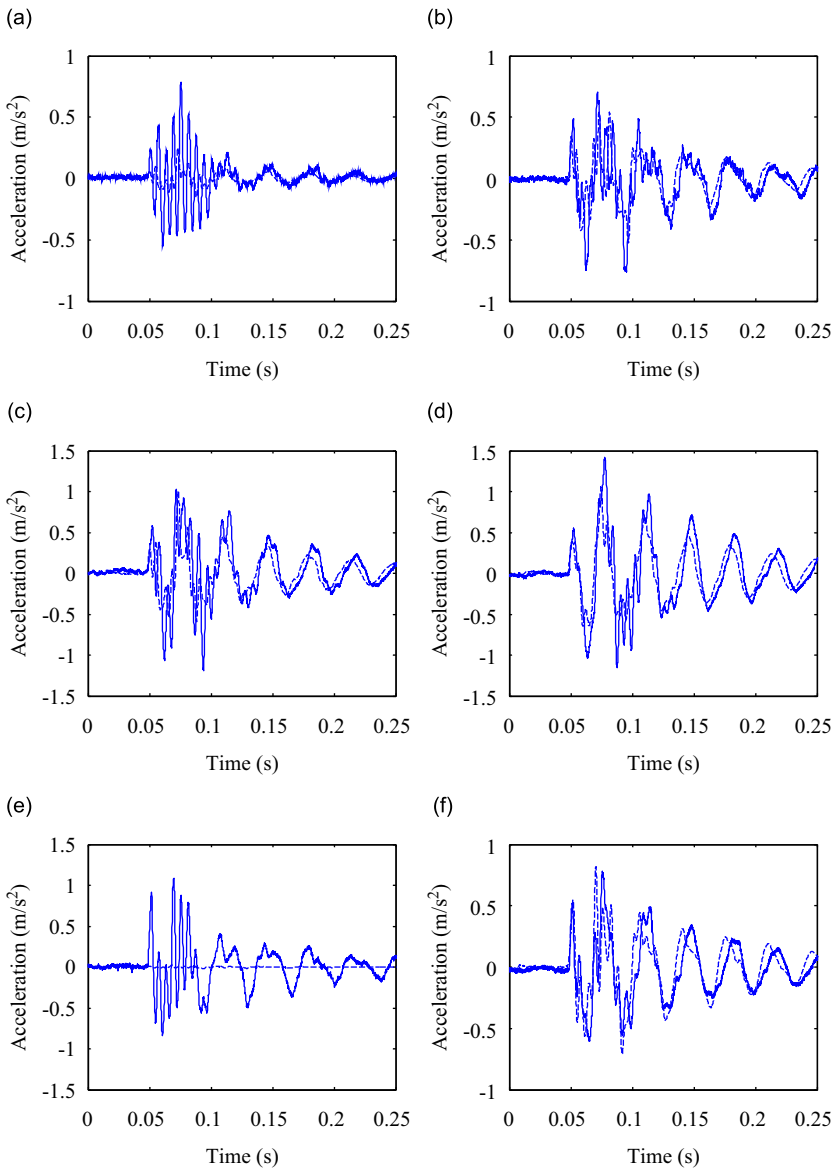


**Fig. 29.** Accelerations on the inside wall surface as a function of time, measured (———) and predicted (- - - - - -), for a sonic boom with duration of 20 ms. Accelerometers (a) 3, (b) 8, (c) 10, (d) 15, (e) 18, and (f) 20.

Time histories and magnitudes of the FFT of the acceleration on the inside wall surface, close to the wall edges (accelerometers 3 and 18), closer to the center of the wall (accelerometers 8 and 10), and the closest to the center of the wall (accelerometers 15 and 20), are shown in Figs. 29 and 30 for the 20-ms N-wave and in Figs. 31 and 32 for the 33.6-ms N-wave, respectively. In the figures, the solid and dashed lines correspond to measured and predicted responses, respectively. Experimental data from accelerometers 3 and 18 indicate that the wall edges vibrate significantly, with a maximum in the frequency near 162 Hz near the top and bottom (e.g. accelerometer 3) and at 28 Hz near the center of the wall vertical edge (e.g. accelerometer 18). At 162 Hz, the wall-mounted microphones close to the top and bottom of the wall exhibited a larger magnitude than the desired spectrum due to imperfections in the method of external pressure generation. The wall edges vibrate because the wall was mounted to the cinderblock cell using brackets, which do not provide a true and continuous simply supported boundary condition. On the other hand, in the model, simply supported boundary conditions impose no displacement on the edges. As a result, the acceleration of the wall is under-predicted near the edges. The discrepancy between experimental and numerical results observed at 162 Hz is caused by the vibration of the of top and bottom edges that it is not captured by the simply supported boundary condition assumed in the model. At other locations, away from the wall edges, numerical predictions are in very good agreement with experimental data, e.g. accelerometers 8, 10, 15, and 20. However, the response remains under-predicted near 162 Hz as a result of the vibration of the wall edges not captured by the model.

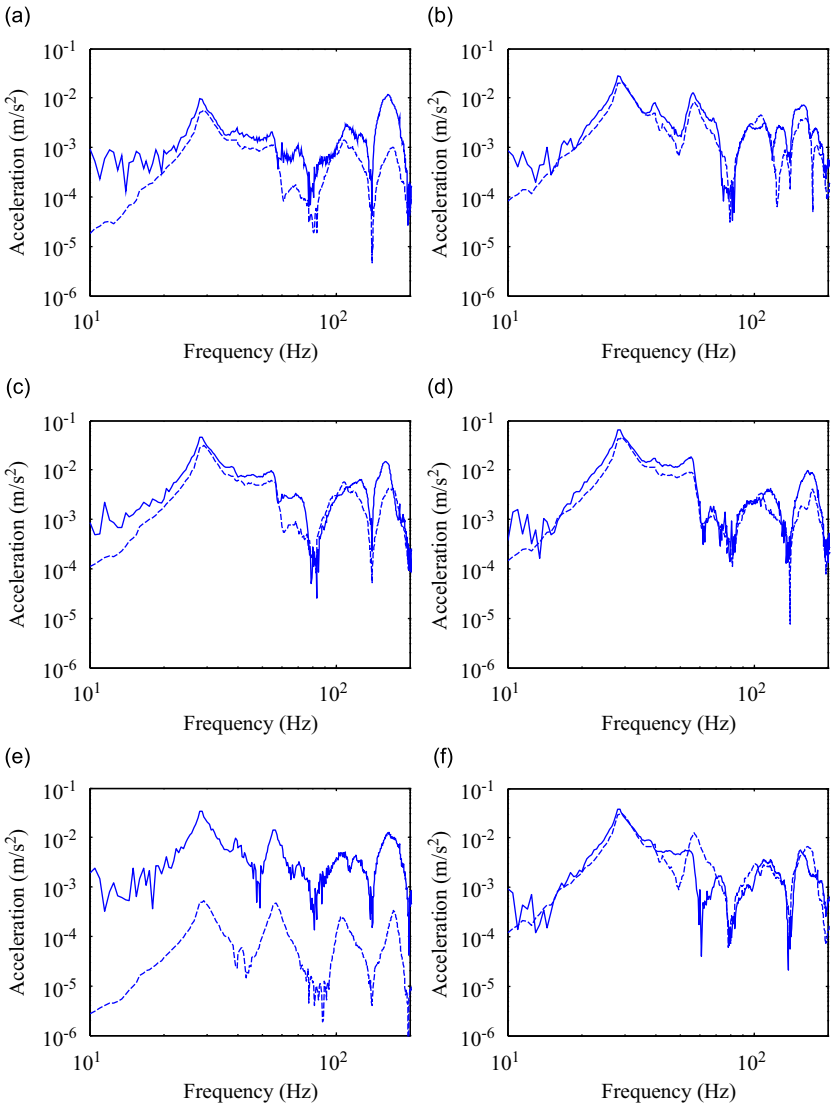


**Fig. 30.** Magnitudes of the FFT of the accelerations on the inside wall surface, measured (———) and predicted (------), for a sonic boom with duration of 20 ms. Accelerometers (a) 3, (b) 8, (c) 10, (d) 15, (e) 18, and (f) 20.

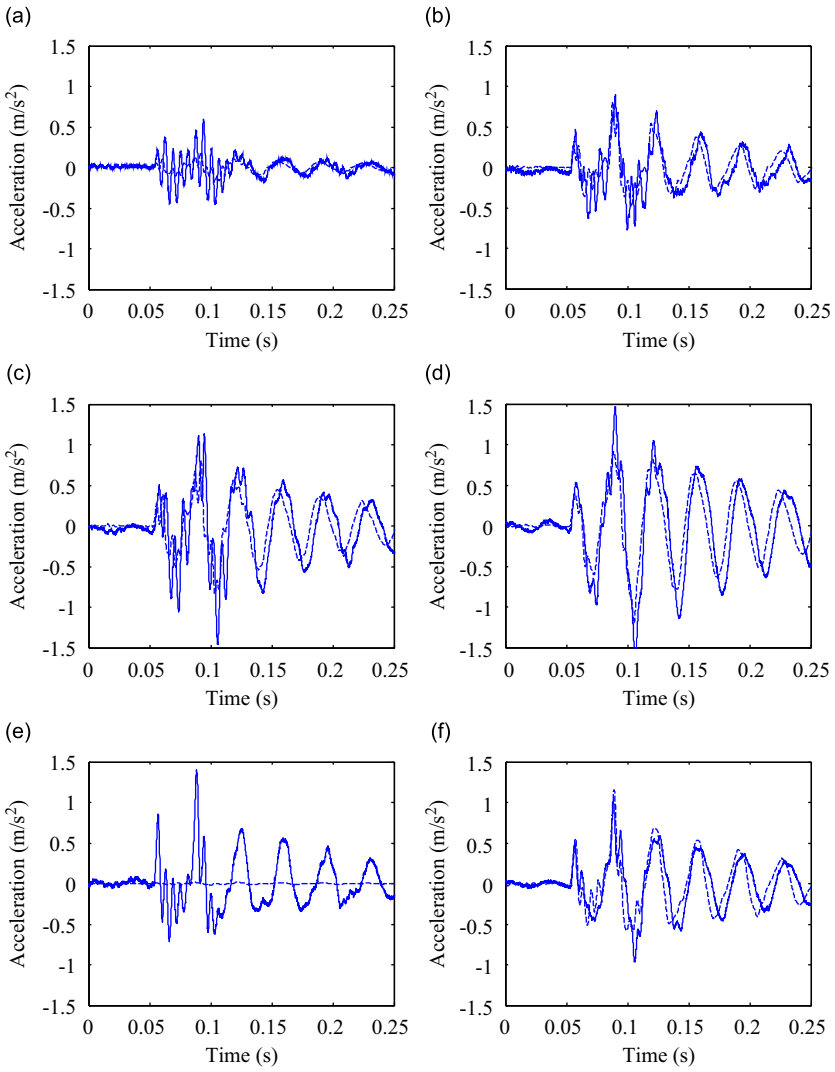


**Fig. 31.** Accelerations on the inside wall surface as a function of time, measured (———) and predicted (------), for a sonic boom with duration of 33.6 ms. Accelerometers (a) 3, (b) 8, (c) 10, (d) 15, (e) 18, and (f) 20.

Figs. 33 and 34 show the time histories (left column) and magnitudes of the FFT (right column) of the pressure close to the center of the wall surface, at the center of the room, and in a corner of the room for N-waves with durations of 20 and 33.6 ms, respectively. In the figures, the solid and dashed lines correspond to measured and predicted responses, respectively. Close to the center of the wall surface, predictions match fairly well the experimental data, which is consistent with the fact that the acceleration is well predicted close to the center of the wall surface. At the center and corners of the room, the model over-predicts the magnitude of the pressure at 28 Hz and under-predicts it at higher frequencies. This is again believed to be due to the vibration of the wall edges that the model does not account for. The contribution to the acoustic response from the edge vibration is likely to be small close to the center of the wall surface and to increase as the observer moves away from the wall (e.g. room center or room corner).

The plaster–wood wall was considered as a uniform orthotropic plate in the prediction model. However, sound is also transmitted through the cavities between the OSB and plaster panels. The mass–air–mass resonance frequency may be expressed as [7],

$$f_0 = \frac{1}{2\pi}\left[\left(\frac{\rho_c c^2}{d}\right)\left(\frac{m_1 + m_2}{m_1 m_2}\right)\right]^{1/2} \tag{26}$$

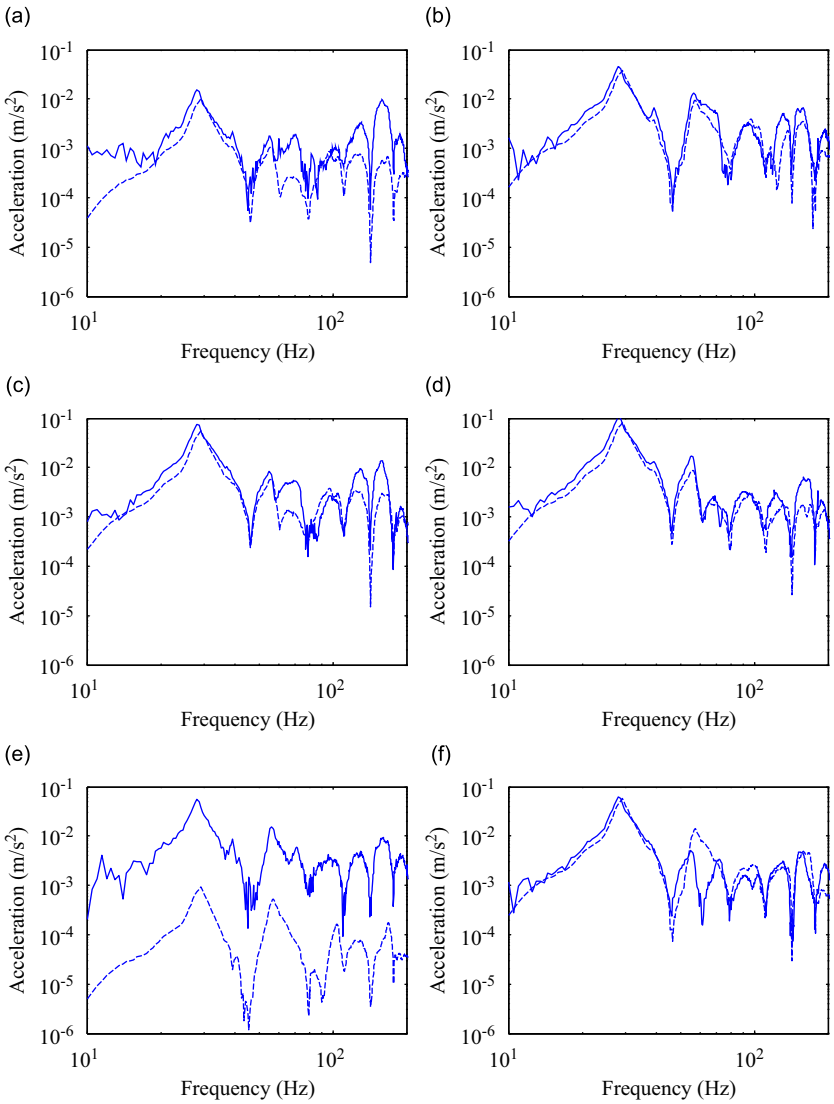


**Fig. 32.** Magnitudes of the FFT of the accelerations on the inside wall surface, measured (———) and predicted (------), for a sonic boom with duration of 33.6 ms. Accelerometers (a) 3, (b) 8, (c) 10, (d) 15, (e) 18, and (f) 20.

where $d$ is the distance between the panels ($d = 8.9$ cm), $\rho_c$ is the density of the fluid in the cavity, $m_1$ and $m_2$ are the respective masses per unit area of the panels (7.6 kg/m$^2$ for OSB and 8.6 kg/m$^2$ for plaster). Assuming that the cavities are filled in with air ($\rho_c = 1.2$ kg/m$^3$), it is found that $f_0 = 100$ Hz. Therefore, around this frequency, it can be expected that more sound will be transmitted into the room cavity than what the model predicts.

## 6. Conclusions

A modal-interaction model was used to predict the vibro-acoustic responses of a rectangular room with one plaster–wood wall exposed to sonic booms. The modal analysis of an illustrative case showed that the structural response is dominated by the fundamental mode with some significant contribution from the third mode. The interior acoustics is dominated by the bulk compressibility of the room. Therefore, a relatively small number of modes are needed to accurately predict the dynamics of the system. It was found that a wave arriving at normal incidence only excites the fully symmetric structural modes. Although some additional modes are excited when the wave arrives at an angle, the wave orientation has

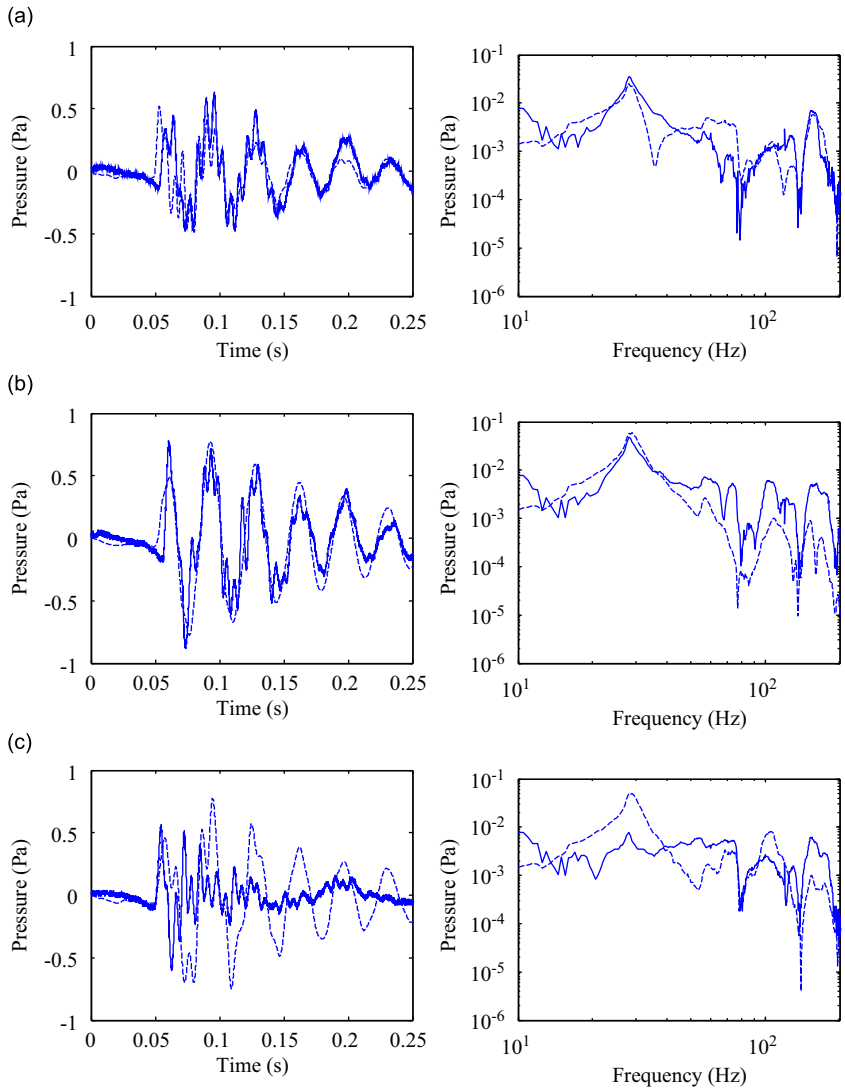


**Fig. 33.** Pressures inside the room, time histories (left) and magnitudes of the FFT (right), measured (———) and predicted (------), for a sonic boom with duration of 20 ms. (a) Close to the center of the wall surface, (b) center of the room, and (c) corner of the room.

virtually no effect on the system response. Vibro-acoustic coupling was found to affect the system response in a significant manner when the first structural mode and the first mode of the pressure anti-symmetric along the directions of the wall have their natural frequency relatively close. Therefore, the fluid–structure interaction needs to be considered as fully coupled for the solution to be truly representative. A parametric study was conducted showing that the amplitudes of the structural and acoustic responses are the largest when the ratio of wave duration and period of the first structural mode is close to unity. It was also found that for integer values of this ratio, the system response exhibits local maxima when vibro-acoustic coupling is weak but does not necessarily follow this trend otherwise.

The vibro-acoustic responses of a cinderblock room with one plaster–wood wall exposed to sonic booms were measured and compared to numerical predictions. Away from the wall edges, predictions of the wall vibration were in good agreement with the experimental data. In the numerical model, the wall was considered as a simply supported orthotropic plate which could not capture the vibration of the wall edges. For the same reasons, room pressure was well predicted close to the center of the wall surface but under-predicted away from the wall surface. The modal-interaction formulation was validated though a more accurate model could potentially be obtained by considering the wall as a plate on elastic rather than simple supports.

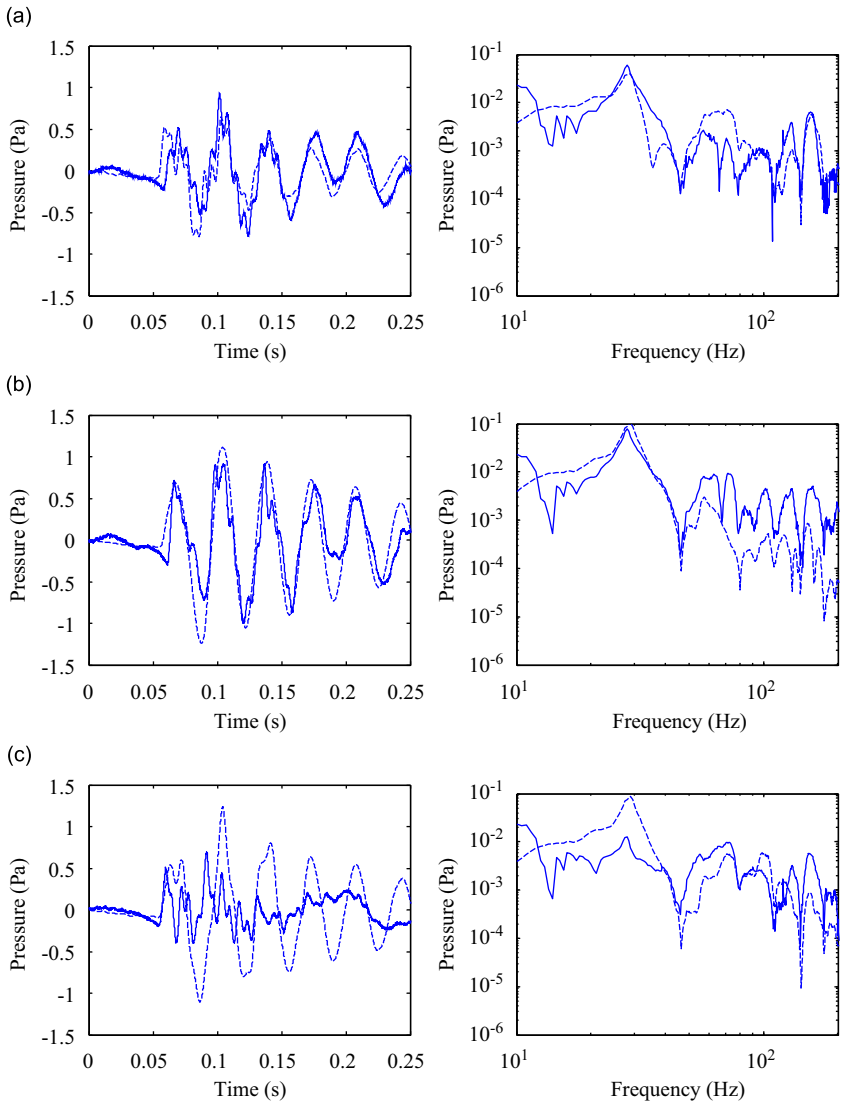


**Fig. 34.** Pressures inside the room, time histories (left) and magnitudes of the FFT (right), measured (———) and predicted (------), for a sonic boom with duration of 33.6 ms. (a) Close to the center of the wall surface, (b) center of the room, and (c) corner of the room.

## Acknowledgments

The authors would like to acknowledge the financial support from NASA Langley Research Center under Grant number NNX07AT36A and its technical monitors Drs. Brenda M. Sullivan and Jacob Klos.

## References

[1] A.J. Pretlove, Free vibrations of a rectangular panel backed by a closed cavity, *Journal of Sound and Vibration* 2 (1965) 197–209.
[2] A.J. Pretlove, Forced vibration of a rectangular panel backed by a closed cavity, *Journal of Sound and Vibration* 3 (1966) 252–261.
[3] A.J. Pretlove, A. Craggs, A simple approach to coupled panel cavity vibrations, *Journal of Sound and Vibration* 11 (1970) 207–215.
[4] N.N. Wahba, Analysis of a plaster–wood wall using a series solution, *Computers & Structures* 35 (1990) 121–140.
[5] N.N. Wahba, Dynamic response of a plaster–wood wall to sonic booms using a series solution, *Computers & Structures* 35 (1990) 141–161.
[6] N.N. Wahba, Analysis of a plaster–wood wall using finite-element method, *Computers & Structures* 36 (1990) 743–753.
[7] F. Fahy, *Sound and Structural Vibration: Radiation, Transmission and Response*, Academic Press, New York, 1985.
[8] A. Tokuyama, K. Sakai, H. Taka, Experimental study of sonic boom acceptance, *AIAA, Aircraft Design, Systems and Operations Meeting*, Monterey, CA, AIAA-1993-3961, August 11–13, 1993.
[9] J.D. Leatherwood, K.P. Shepherd, B.M. Sullivan, A new simulator for assessing subjective effects of sonic booms, NASA-TM-104150, 1991.
[10] J.D. Leatherwood, B.M. Sullivan, Laboratory study of effects of sonic boom shaping on subjective loudness and acceptability, NASA-TP-3269, 1992.
[11] J. Salamone, Sonic boom simulation using conventional audio equipment, *Noise-Control 2004*, Baltimore, MD, 2004.

[12] Y. Naka, Y. Makino, T. Ito, Laboratory experiment on indoor sonic booms and sonic-boom-induced vibration of buildings, in: *14th AIAACEAS Aeroacoustics Conference*, Vancouver, BC, Canada, AIAA-2008-3037, May 5–7, 2008.
[13] S.M. Dickinson, The buckling and frequency of flexural vibration of rectangular, isotropic and orthotropic plates using Rayleigh's method, *Journal of Sound and Vibration* 61 (1978) 1–8.
[14] A.D. Pierce, *Acoustics: An Introduction to its Physical Principles and Applications*, McGraw-Hill, New York, 1991.
[15] N.N. Wahba, I.I. Glass, R.C. Tennyson, Pressures inside a room subjected to simulated sonic booms, *Journal of Sound and Vibration* 68 (1980) 259–279.
[16] A. Edward, R. Thallon, *Fundamentals of Residential Construction*, Wiley, New York, 2006.
[17] D.J. Ewins, *Modal Testing, Theory, Practice and Application*, Research Studies Press Ltd., 2000.